MODELING OF PERFORMANCE BEHAVIOR IN GAS CONDENSATE RESERVOIRS USING A VARIABLE MOBILITY CONCEPT

A Thesis

by

BENTON WADE WILSON

Submitted to the Office of Graduate Studies of
Texas A&M University
in partial fulfillment of the requirements for the degree of

MASTER OF SCIENCE

December 2003

Major Subject: Petroleum Engineering

MODELING OF PERFORMANCE BEHAVIOR IN GAS CONDENSATE RESERVOIRS USING A VARIABLE MOBILITY CONCEPT

A Thesis

by

BENTON WADE WILSON

Submitted to the Office of Graduate Studies of
Texas A&M University
in partial fulfillment of the requirements for the degree of

MASTER OF SCIENCE

Approved as to style and content by:

Thomas A. Blasingame (Chair of Committee)	W. John Lee (Member)
Robert R. Berg (Member)	Hans C. Juvkam-Wold (Interim Head of Department)

December 2003

Major Subject: Petroleum Engineering

ABSTRACT

Modeling of Performance Behavior in Gas Condensate Reservoirs
Using a Variable Mobility Concept. (December 2003).
Benton Wade Wilson,
B.S., Georgia Institute of Technology
Chair of Advisory Committee: Dr. Thomas A. Blasingame

The proposed work provides a concept for predicting well performance behavior in a gas condensate reservoir using an empirical model for gas mobility. The proposed model predicts the behavior of the gas permeability (or mobility) function in the reservoir as condensate evolves and the gas permeability is reduced in the near-well region due to the "condensate bank". The proposed model is based on observations of simulated reservoir performance and predicts the behavior of the gas permeability over time and radial distance. This model is given by:

$$k = k_{min} + (k_{max} - k_{min}) \left[1 - \exp\left[\frac{-1}{\alpha} \frac{r^2}{t} \right] \right]$$

The proposed concept has potential applications in the development of a pressure-time-radius solution for gas condensate reservoirs experiencing this type of mobility behavior. We recognize that the proposed concept (*i.e.,* a radially-varying gas permeability) is oversimplified, in particular, it ignores the diffusive effects of the condensate (*i.e.,* the viscosity-compressibility behavior). However, we have effectively validated the proposed model using literature results derived from numerical simulation.

This new solution is presented graphically in the form of "type curves." We propose that the "time" form of this solution be used for applications in well test analysis. Previous developments used for the analysis of well test data from gas condensate reservoirs consider the *radial composite* reservoir model, which utilizes a "step change" in permeability at some radial distance away from the wellbore. Using our proposed solution we can visualize the effect of the varying gas permeability in time and radius (a suite of (dimensionless) radius and time format plots are provided). In short, we can visualize the evolution of the condensate zone as it evolves in time and radial distance.

A limitation is the simplified form of the k_g profile as a function of radius and time — as well as the dependence/appropriateness of the α-parameter. While we suspect that the α-parameter represents the influence of both fluid and rock properties, we do not examine how such properties can be used to calculate the α-parameter.

DEDICATION

My wife Moya, and three children, Brittany, Colton, and Colby
Thank you for the support and unconditional love.

My family, past and present,
whom all have either worked in the oilfield
or have been married to it.

My father, Jack Wilson,
and the many talks we have had "completing a well".

ACKNOWLEDGEMENTS

I would like to express my appreciation and sincerely thank the following:

Dr. Tom Blasingame, chair of my advisory committee — for his unique mix of intellect and practicality in his work, which I highly admire. Also, my deep gratitude for his friendship, patience and willingness to share his knowledge, time, and experience with myself and others. Thank you for the strong commitment to our research.

Dr. Rosalind Archer — for enthusiasm in her teaching, as well as her patience and ability to make difficult topics much clearer. My sincerest gratitude and admiration for her light-hearted personality and her extensive knowledge. Thank you for the valuable assistance with this research.

Dr. John Lee — for his sharing of experiences and knowledge through his teaching and published works, and for serving as a member on my advisory committee.

Dr. Bob Berg — for serving as a member of my advisory committee

The Nuclear Technology group at Baker Hughes, particularly Dr. Darryl Trcka, Dr. Allen Gilchrist, and Dr. Alan McFall, as well as Dr. Don Oliver and Dr. Medhat Mickael, both who have pursued other paths from Baker Hughes — for support in my career, patience, and belief in my abilities.

Baker Hughes, Inc. for providing the support, time, and financial backing to make this endeavor possible.

TABLE OF CONTENTS

Page

CHAPTER I INTRODUCTION 1
1.1 Research Problem 1
1.2 Research Objectives 4
1.3 Statement of the Problem and Summary of a Proposed Solution 5
1.4 Outline of Thesis 10

CHAPTER II LITERATURE REVIEW 12
2.1 Radial Composite Reservoir System 12
2.2 General Concepts – $p(r,t)$ Performance in Gas Condensate Reservoirs 13
2.3 Other Solutions/Considerations 14

CHAPTER III DEVELOPMENT OF AN ANALYTICAL PRESSURE SOLUTION FOR THE CASE OF A PERMEABILITY PROFILE THAT VARIES IN TIME AND RADIAL DISTANCE 18
3.1 Concept of a Mobility Profile that Varies in Time and Radial Distance 18
3.2 Application of the Boltzmann Transformation to the Radial Diffusivity Equation – Development of the Pressure Derivative Solutions 19
3.3 Wellbore Storage and Skin Effects 23

CHAPTER IV VALIDATION OF AN ANALYTICAL PRESSURE SOLUTION FOR THE CASE OF A PERMEABILITY PROFILE THAT VARIES IN TIME AND RADIAL DISTANCE – GAS CONDENSATE RESERVOIRS 31
4.1 Comparison of the New Solution and Solutions for the Sealing Faults and Radial Composite Reservoir Cases 31
4.2 Validation of the New Solution – Literature Data 34

CHAPTER V SUMMARY, CONCLUSIONS, AND RECOMMENDATIONS FOR FUTURE WORK 45
5.1 Summary 45
5.2 Conclusions 45
5.3 Limitations and Recommendations 47

NOMENCLATURE 48

REFERENCES 50

Page

APPENDIX A DERIVATION OF THE PRESSURE DERIVATIVE FUNCTIONS WITH RESPECT TO TIME AND RADIUS FOR THE CASE OF A RADIALLY VARYING PERMEABILITY PROFILE (EQUIVALENT LIQUID CASE) 52

APPENDIX B AN APPROXIMATE TECHNIQUE FOR THE DIRECT ADDITION OF WELLBORE STORAGE AND SKIN EFFECTS 66

APPENDIX C A QUADRATIC FORMULA FOR NUMERICAL DIFFERENTIATION 67

VITA 68

LIST OF FIGURES

FIGURE Page

1.1 Schematic diagram of gas condensate (liquid) behavior as a function of distance in the reservoir (after Roussennac[1]) 3

1.2 Gas mobility profiles for a gas condensate reservoir system (as a function of time and radius) (adapted from Roussennac[1]) 5

1.3 "Type curve" representation of the new model ($p_D(\varepsilon_D)$ formulation (Eq. 1.5)). Solution is plotted versus the modified Boltzmann transform variable ($r_D^2/(\alpha_D t_D)$). 8

1.4 "Type curve" representation of the new model ($|r_D\, dp_D/dr_D|$ formulation (Eq. 1.6)). Solution is plotted versus the modified Boltzmann transform variable ($r_D^2/(\alpha_D t_D)$). 9

1.5 "Type curve" representation of the new model ($t_D(\partial p_D/\partial t_D)$ formulation (Eq. 1.6)). Solution is plotted versus the inverse of the modified Boltzmann transform variable ($(\alpha_D t_D)/r_D^2$). 9

2.1 Dimensionless pressure type curve for radial flow behavior including wellbore storage and skin effects (p_{wD} versus t_D/C_D format). This plot presents a comparison of the solution generated using numerical inversion (as a surrogate for the exact solution) and the approximate solution technique proposed in ref. 16 and generated using *Mathematica*. 15

2.2 Dimensionless pressure derivative type curve for radial flow behavior including wellbore storage and skin effects (p_{wD}' versus t_D/C_D format). This plot presents a comparison of the solution generated using numerical inversion (as a surrogate for the exact solution) and the approximate solution technique proposed in ref. 16 and generated using *Mathematica*. 16

FIGURE Page

2.3 Pressure derivative type curve for a vertical well producing at a constant rate near a sealing fault in a homogeneous, infinite-acting reservoir. 16

2.4 Pressure derivative type curve for a vertical well producing at a constant rate in a composite radial system, various mobility (λ)/storativity (ω) cases. 17

3.1 Gas mobility profiles for a gas condensate reservoir system (as a function of time and radius) (adapted from Roussennac[1]) — note the comparison of the simulated performance and the proposed models (*i.e.*, the exp(x) and the erf (x) mobility models). 18

3.2 "Type curve" representation of the $p_D(\varepsilon_D)$ solution (Eq. 3.12)). Solution is plotted versus the modified Boltzmann transform variable $(r_D^2/(\alpha_D t_D))$. 21

3.3 "Type curve" representation of the $|\varepsilon_D\, dp_D/d\varepsilon_D|$ solution (Eq. 3.11)). Solution is plotted versus the modified Boltzmann transform variable $(r_D^2/(\alpha_D t_D))$. 22

3.4 "Type curve" representation of the new model ($|r_D\, dp_D/dr_D|$ formulation (Eq. 1.6)). Solution is plotted versus the modified Boltzmann transform variable $(r_D^2/(\alpha_D t_D))$. 22

3.5 "Type curve" representation of the new model ($t_D(\partial p_D/\partial t_D)$ formulation (Eq. 1.6)). Solution is plotted versus the inverse of the modified Boltzmann transform variable $((\alpha_D t_D)/r_D^2)$. 23

3.6a Dimensionless pressure type curve for radial flow behavior including wellbore storage and skin effects (p_{wD} versus t_D/C_D format). This plot presents a comparison of the solution generated using numerical inversion (as a surrogate for the exact solution) and the approximate solution technique proposed in ref. 16 and generated using *Mathematica*. 25

FIGURE Page

3.6b Dimensionless pressure derivative type curve for radial flow behavior including wellbore storage and skin effects (p_{wD}' versus t_D/C_D format). This plot presents a comparison of the solution generated using numerical inversion (as a surrogate for the exact solution) and the approximate solution technique proposed in ref. 16 and generated using *Mathematica*. 25

3.7a Type curve plot (p_{wD} and p_{wD}' versus t_D/C_D) — $C_D = 1\text{x}10^3$, $\alpha_D = 1\text{x}10^0$, various k_{min}/k_{max} cases. 27

3.7b Type curve plot (p_{wD} and p_{wD}' versus t_D/C_D) — $C_D = 1\text{x}10^3$, $\alpha_D = 1\text{x}10^{-1}$, various k_{min}/k_{max} cases. 27

3.7c Type curve plot (p_{wD} and p_{wD}' versus t_D/C_D) — $C_D = 1\text{x}10^3$, $\alpha_D = 1\text{x}10^{-2}$, various k_{min}/k_{max} cases. 28

3.7d Type curve plot (p_{wD} and p_{wD}' versus t_D/C_D) — $C_D = 1\text{x}10^3$, $\alpha_D = 1\text{x}10^{-3}$, various k_{min}/k_{max} cases. 28

3.7e Type curve plot (p_{wD} and p_{wD}' versus t_D/C_D) — $C_D = 1\text{x}10^3$, $\alpha_D = 1\text{x}10^{-4}$, various k_{min}/k_{max} cases. 29

3.7f Type curve plot (p_{wD} and p_{wD}' versus t_D/C_D) — $C_D = 1\text{x}10^3$, $\alpha_D = 1\text{x}10^{-5}$, various k_{min}/k_{max} cases. 29

3.8 Drawdown type curve plot (p_{wD}' versus t_D/C_D) — $C_D = 1\text{x}10^3$, $\alpha_D = 1\text{x}10^0, 10^{-1}, 10^{-2}, 10^{-3}, 10^{-4}, 10^{-5,}$ various $k_{min}/k_{max} = 1\text{x}10^0, 10^{-1}, 10^{-2}, 10^{-3}$. 30

3.9 Drawdown type curve plot (p_{wD}' versus t_D/C_D) — $C_D = 1\text{x}10^{20}$, $\alpha_D = 1\text{x}10^0, 10^{-1}, 10^{-2}, 10^{-3}, 10^{-4}, 10^{-5,}$ various $k_{min}/k_{max} = 1\text{x}10^0, 10^{-1}, 10^{-2}, 10^{-3}$. 30

4.1 Pressure derivative type curve for a vertical well producing at a constant rate near a sealing fault in a homogeneous, infinite-acting reservoir. 31

FIGURE Page

4.2 Pressure derivative type curve for a vertical well producing at a constant flowrate in a 2-zone radial composite reservoir system, various mobility (λ)/storativity (ω) cases. 32

4.3 Combined pressure derivative type curve for the following cases: sealing faults, a single radial composite region, and the proposed model for a radially-varying mobility profile. 33

4.4a z-factor profiles for the Roussennac[1] data case (Mix 2) — includes Roussennac EOS (simulation) data and data from dry gas correlation. 35

4.4b Gas viscosity profiles for the Roussennac[1] data case (Mix 2) — includes Roussennac EOS (simulation) data and data from dry gas correlation. 35

4.4c Pseudopressure trend for the Roussennac[1] data case (Mix 2) — generated using the z-factor and gas viscosity data obtained from the dry gas correlations, and the pseudopressure definition given by Eq. 4.01. 36

4.5 p_p versus r for the Roussennac case of Fig. 2.7 — the pressure data were digitized and later converted to pseudopressure (p_p) using the transformation shown in **Fig. 4.4c**. 37

4.6 Example case of p versus r for liquid flow — presented by Lee (ref. 18). 37

4.7 Δp_p and $|\eta\, d\Delta p_p/d\eta|$ functions versus η for Roussennac Fig. 2.7 ($\eta=r^2/t$). The scatter in the $|\eta\, d\Delta p_p/d\eta|$ function is due to the Δp_p data not being uniquely "line source" in character (*i.e.*, these are numerical simulation results, and are not bound to the "line source" criterion). 38

4.8 Δp_p and $|\eta\, d\Delta p_p/d\eta|$ functions versus η ($\eta=r^2/t$) (data from Roussennac Fig. 2.7, model trends are derived from the new model for a varying mobility profile). 38

FIGURE Page

4.9a Match of Roussenac[1] data (digitized) and the new variable mobility model (type curve match) — $p_D(\varepsilon_D)$ versus $(\alpha_D t_D)/r_D^2$ format..... 40

4.9b Match of Roussenac[1] data (digitized) and the new variable mobility model (type curve) — $|r_D(\partial p_D/\partial t_D)|$ versus $(\alpha_D t_D)/r_D^2$ format..... 41

4.10 Match of Roussenac[1] data (digitized) and the new variable mobility model (data/model match) — Δp and $r|dp/dr|$ versus r^2 format..... 41

4.11a z-factor profiles for the Vo[19] data case (Fluid 2) — Vo EOS (simulation) data..... 42

4.11b Gas viscosity profiles for the Vo[19] data case (Fluid 2) — Vo EOS (simulation) data..... 42

4.11c Pseudopressure trend for the Vo[19] data case (Fluid 2) — generated using the z-factor and gas viscosity data obtained from Vo EOS calculations, and the pseudopressure definition given by Eq. 4.01..... 43

4.12 Match of Vo[19] data (digitized) and the new variable mobility model (data/model match) — Δp_p and $\varepsilon|d\Delta p_p/d\varepsilon|$ versus η ($\eta = r^2/t$) format. (s=0)..... 44

CHAPTER I
INTRODUCTION

1.1 Research Problem

During the production of a gas reservoir, the associated pressure history can be used to estimate reservoir properties and provide insight into well performance versus expectations. This pressure history, however; may be difficult to categorize. Not only does the performance of a gas reservoir (and particularly, a gas condensate reservoir) exhibit various types of depletion performance, but geological complexities (such as faults and permeability variation) also yield variations in the production-pressure history. When combined, such effects are very difficult to "uncouple" and may actually be indistinguishable from one another (*e.g.*, the solutions for a radial composite system and a sealing fault(s) can be very similar to one another (even indistinguishable in extreme cases (such as a single sealing fault)).

Well testing is the primary means for establishing the presence of such features as gas condensate performance effects, geological structures, etc — however, we must recognize that the problem of "uniqueness" is perhaps the most difficult to overcome, and conventional analysis/interpretation techniques may not be sufficient to properly characterize such effects. Hence, it is the motivation for this work that we establish a new solution for the transient drawdown performance of gas condensate reservoirs.

We note that the current approach of using reservoir simulation to resolve such issues is more flexible than the traditional well test analysis methods — however, the detail at which reservoir simulation is performed may not address the physical phenomena being observed in the performance data. Simulation can be scaled as finely or as coarsely as desired — but how does one "calibrate" the numerical model to the physical problem without making limiting assumptions? On the other hand, an analytic (or semi-analytic) solution is also simplified to fit conditions where it can be solved, but such solutions provide insight into the *characteristic behavior* of the system.

The behavior of gas condensate reservoir systems can be difficult to model and predict. Specifically, in many areas (*e.g.*, the North Sea) the question often arises as to whether an unexpected decline in gas production is a result of depletion, or if this is a result of condensate banking. Liquid condensate develops as reservoir pressure declines below the dewpoint pressure — and the degree to which this occurs depends on many factors such as the composition of the gas, and the reservoir conditions. Liquid condensate will impede the flow of the gas phase, restricting production flowrate and adversely affecting recovery.

This thesis follows the style and format of the *SPE Journal*.

Examination of differential pressure data plotted with respect to radial distance from the wellbore (generated using numerical simulation) will indicate *the possibility* of condensate banking. Roussennac[1] proposes that three regions (or zones) typically exist in a gas condensate reservoir system — these regions are described by Roussennac (and Fevang, as referenced by Roussennac) as follows:

- Region 1 — Condensate Bank: By definition, this region near the wellbore has a condensate (oil) saturation that is high enough to permit the condensate fluid to flow. Obviously, the reservoir pressure in this area is the lowest of the three regions. As noted by Roussennac, the overall composition of the flowing mixture in this region is essentially constant in this area (as indicated by a near constant *GOR*) and is approximately the same composition as the single phase gas at the boundary of Region 1 and Region 2. The specific criteria used to characterize the condensate phase is that there is condensate flow in Region 1 (although the evolution of this "mobile" condensate is thought to be the boundary section for Regions 1 and 2.

  As shown schematically in **Fig. 1.1**, the oil saturation decreases as radial distance from the wellbore increases — that is, the distribution of fluids near the well is relatively stable — "drying" to essentially the original dry gas at distances from the wellbore. Fig. 1.1 suggests that there is a "condensate" gradient in the near-well region, but that the gradient in this region is substantially less than the one experienced in "Region 2" (*i.e.*, the "condensate buildup" or "transition" zone). This concept (validated by numerical simulation) suggests that Region 1 can be treated as a simple two-phase region with constant phase mobilities. On the other hand, Region 2 is seen as a region of rapid change in condensate saturation.

- Region 2 — Condensate Buildup Zone: This region differs from Region 1 in that the condensate is believed to have a low mobility and while it will establish a gradient or transition zone, the condensate will not tend to flow. The outer edge of Region 2 is the point some radial distance from the well where the first droplets of liquid evolve from the gas phase — therefore, the pressure at this particular distance (which does continue to propagate) is the dewpoint pressure of the original reservoir gas.

  As noted by Roussennac, the gas phase composition "leans out" in Region 2, with the heavier components being evolved as condensate. This phenomenon continues as we approach the wellbore and the gas "leans out" to a minimum richness at the wellbore. It is worth noting that the condensate saturation is substantially lower in Region 2 than Region 1, which does (conceptually) permit us to consider Region 2 to be a single-phase gas region for the purpose of well testing (in some cases). Roussennac (and others) have utilized the 3-region concept for the analysis of well test data from gas condensate reservoirs with the objective of characterizing each region using a 3-zone radial composite reservoir model. There are varying degrees of success with this concept, and many analysts prefer using only a 2-zone model, while other analysts insist that the 3-zone model is more appropriate.

Finally, we repeat the premise that only gas is flowing in Region 2 — therefore, the intermediate and heavier components evolve as condensate near the boundary of Regions 1 and 2. This provides the condensate which forms the "bank" in Region 1.

- Region 3 — Original Dry Gas Region: By definition, no condensate exists in this region — only the gas phase is present (*i.e.*, the pressure is greater than the dewpoint pressure).

We note that the prevailing wisdom is that all three regions exist in a typical gas condensate reservoir. Region 1 is likely to exist when $p_{res}<p_{dew}$ and Region 2 will always exist if Region 1 exists (*i.e.*, there must be a condensate gradient region). Region 3 exists during transient flow behavior, and if outer boundaries are encountered then the reservoir pressure may drop below p_{dew}, and Region 3 (*i.e.*, the original dry gas state may not exist).

Roussennac suggests that Region 2 may become negligible for the case of a very rich gas or near critical gas condensate fluids. This phenomenon can be modeled with PVT experiments — however, if this behavior existed, it would be difficult to distinguish from other conditions. We believe that the "concept" of 3 regions is relevant (and perhaps appropriate) for many cases. Roussennac has proposed a schematic diagram for this process (see **Fig. 1.1**) and we agree with this proposal as for as the reservoir processes, we are less certain regarding well test analyses — but we acknowledge that, conceptually, **Fig. 1.1** validates the application of the 2 or 3-zone radial composite reservoir model for the analysis of well test data obtained from gas condensate reservoirs.

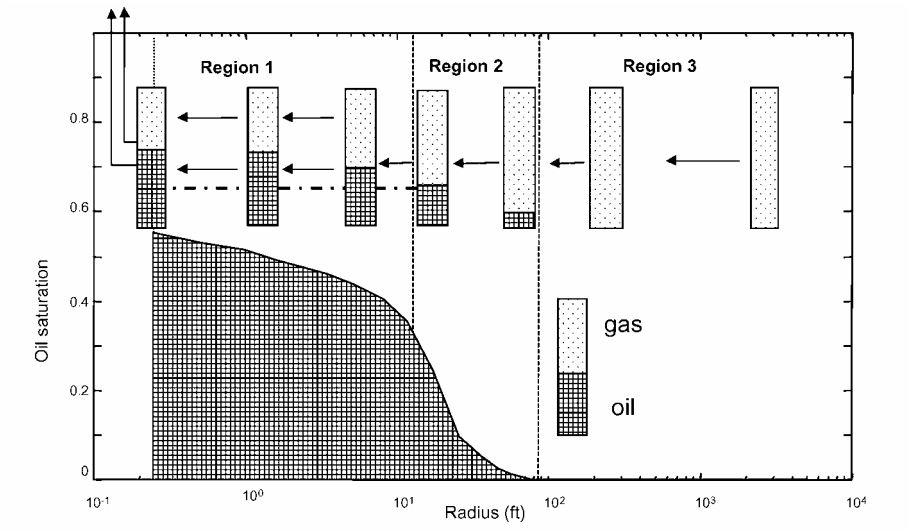

Figure 1.1 – Schematic diagram of gas condensate (liquid) behavior as a function of distance in the reservoir (after Roussennac[1]).

We also believe that applications in actual reservoirs will differ somewhat from the results of such "idealized" studies — in particular, a gas condensate reservoir may not exhibit the expected condensate

bank and/or there could be other reservoir characteristics (*e.g.*, geologic features) that impair or complicate the analysis/interpretation of reservoir performance data from gas condensate reservoirs. The economic aspects of this situation are relevant as well — future development strategies depend on a representative characterization of the reservoir in question. This is one aspect of our motivation to address the problem of variable mobility profile directly using a solution which explicitly incorporates this behavior.

Our proposed solution involves the identification of (liquid) condensate development with respect to time and distance from the well. We present distinctive solutions in the form of "type curves" that can be used to visually identify condensate evolution in terms of mobility behavior with respect to time and radius. These type curves are developed using a new solution for the case of a changing effective permeability (or mobility) as a function of dimensionless time and dimensionless radius and are presented in three formats: a unified variable based on the dimensionless Boltzmann transform variable ($r_D^2/(4t_D)$), dimensionless radius (r_D), and dimensionless time(t_D). As we cannot measure pressure in the reservoir, the only practical tool for well test analysis is the family of type curves given in the dimensionless time (t_D) format.

1.2 Research Objectives

The primary objectives of this work are:

- To develop an analytical representation of the pressure behavior in time and space for a reservoir system with a varying mobility profile (see **Fig. 1.2** for a schematic of a varying mobility profile for a gas condensate reservoir system). The concept is based on an empirical model for the gas mobility function. The model considers a varying gas permeability that assigns the maximum gas permeability for the condition where only gas (no condensate) is present in the reservoir. The minimum gas permeability is the value at the condition where the mobility of the gas has been impeded by maximum condensate dropout. This mobility model is given as:

$$k = k_{min} + (k_{max} - k_{min})\left[1 - \exp\left[\frac{-1}{\alpha}\frac{r^2}{t}\right]\right] \quad \text{.....(1.1)}$$

  The concept is based on the observation of minimum gas permeability (or mobility) near the wellbore and the maximum (original) gas permeability in the "dry gas" portion of the reservoir. The model predicts the permeability behavior during the transition regime between the two extreme maximum and minimum permeability values. The model was constructed after considering observations made from numerical simulation results where saturation, effective permeability, and gas mobility are presented as functions of distance in the reservoir.

The secondary objectives of this work are:

- To utilize this new model as a mechanism to develop graphical solutions for the pressure derivative in time and radial distance. This solution can be compared to other solutions (*e.g.*, the 2 (or 3)-zone radial composite reservoir model and various cases of the sealing fault model (time derivative), as well as the pressure and pressure derivative (radial derivative) as a function of radial distance derived from numerical simulation).
- To use this model for the analysis of well test data from gas condensate reservoirs with the intention of developing solutions which include wellbore storage and skin effects.
- To propose applications for the analysis of well test data acquired from pressure drawdown or pressure buildup tests.

1.3 Statement of the Problem and Summary of a Proposed Solution

This work is focused on the concept of using a functional form for the gas mobility profile (*i.e.*, k/μ) and incorporating an empirically-derived model into the rigorous diffusivity equation for the liquid case.

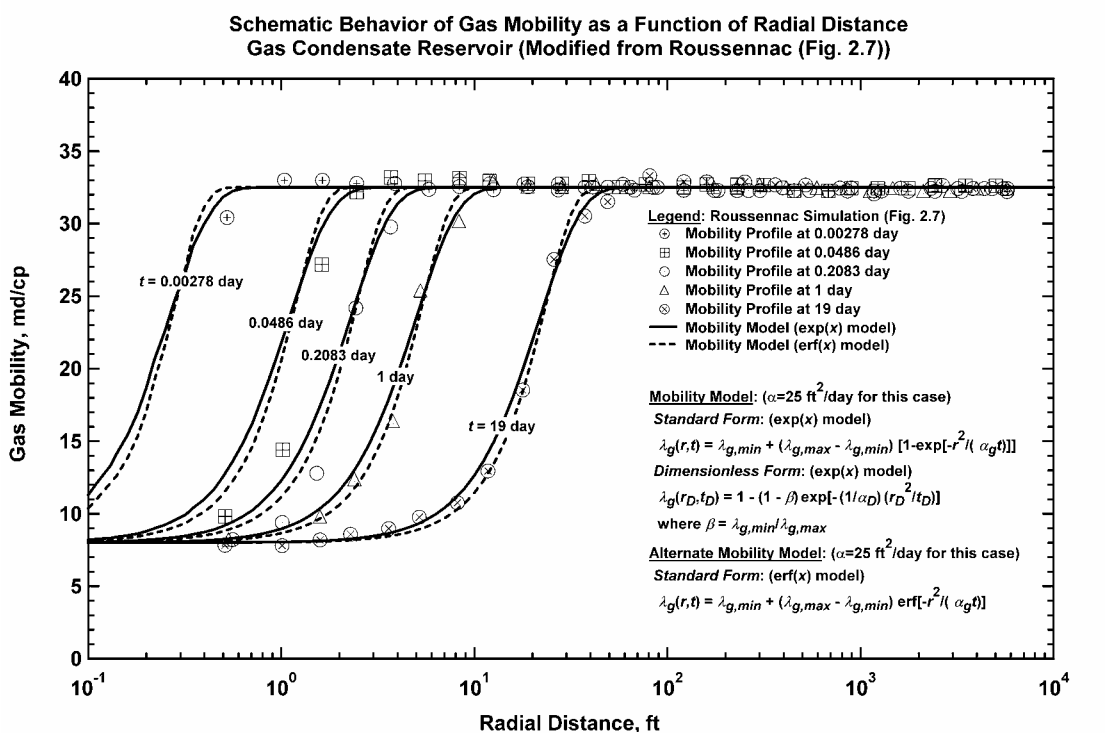

Figure 1.2– Gas mobility profiles for a gas condensate reservoir system (as a function of time and radius) (adapted from Roussennac[1]) — note the comparison of the simulated performance and the proposed models (*i.e.*, the exp(x) and the erf (x) mobility models).

We wish to use this concept and the resulting flow model to represent the pressure behavior of the gas condensate case with respect to time and radial distance from the wellbore. We treat this case as "liquid equivalent," where we consider non-idealities (*e.g.,* pressure-dependent PVT functions) by using the conventional pseudofunctions (*i.e.* pseudopressure and pseudotime).

We have used the simulation cases presented by Roussennac[1] as a starting point for establishing a model for gas mobility behavior as a function of radius and time for a gas condensate reservoir. We recognize that simulated profiles are problematic (*i.e.*, a different set of input data may yield a different profile), but we believe that the cases presented by Roussennac offer an appropriate starting point as these cases are well calibrated and verified

Using the results presented by Roussennac (see **Fig. 1.2**), we have established the following *conceptual* model for representing the gas permeability as a function of radius and pressure:

$$k = k_{min} + (k_{max} - k_{min}) \left[1 - \exp\left[\frac{-1}{\alpha} \frac{r^2}{t} \right] \right] \quad \text{("exponential" or exp(}x\text{) model)} \ldots\ldots\ldots\ldots\ldots\ldots (1.2)$$

We also compare the exponential model with the following erf(x) model:

$$k = k_{min} + (k_{max} - k_{min}) \ \text{erf}\left[-\frac{r^2}{\alpha t} \right] \quad \text{("error function" or erf(}x\text{) model)} \ldots\ldots\ldots\ldots\ldots\ldots (1.3)$$

For the purposes of this work we will use the form given by Eq. 1.1 (*i.e.*, the exp(x) model) and presume a "liquid equivalent case" (*i.e.*, k is simply a function of radius and time (not explicitly a function of pres-sure)). The definition of the diffusivity equation for this case is given as:

$$\frac{1}{r} \frac{\partial}{\partial r} \left[k\, r \frac{\partial p}{\partial r} \right] = \frac{1}{0.0002637} \phi \mu c_t \frac{\partial p}{\partial t} \ \text{(Field units)} \ldots\ldots\ldots\ldots\ldots\ldots (1.4)$$

Eq. 1.2 is used as the permeability model, and is coupled with the radial flow diffusivity equation for this case (*i.e.*, Eq. 1.4). We assume a well in an infinite-acting radial flow system produced at a constant flowrate, and, as noted earlier, we specifically assume that permeability is an explicit function of radius and time $k=f(r,t)$. In order to solve the resulting differential equation, we use the Boltzmann transformation (based on the appropriate definition of dimensionless variables) (see Appendix A).

We provide different forms of the solution — forms in terms of the Boltzmann variable $(\varepsilon_D = r_D^2 / 4t_D)$, as well as the dimensionless pressure and the dimensionless pressure derivative functions in terms of the dimensionless radius and time variables. These forms will prove useful for different applications — the radial distance forms are useful for validation of the new solution with reservoir simulation results, while the time forms of the solution will have utility in the analysis of well test and production data.

"Pressure Solution"

$$p_D = \frac{1}{2}\left[k_{\min}/k_{\max}\right]^{\frac{\alpha_D}{4}} * \int_{\varepsilon_D}^{\infty} \left[\frac{1}{\varepsilon_D} \exp\left[-\frac{\left[1+\frac{4}{\alpha_D}\right]}{\frac{4}{\alpha_D}} \ln\left[e^{-\frac{4}{\alpha_D}\varepsilon_D} - (1-k_{\min}/k_{\max})\right] + \frac{4}{\alpha_D}\varepsilon_D \right] \right] d\varepsilon_D \quad \text{.....(1.5)}$$

"Pressure Derivative in Time"

$$t_D \frac{\partial p_D}{\partial t_D} = \frac{1}{2}\left[k_{\min}/k_{\max}\right]^{\frac{\alpha_D}{4}} * \exp\left[-\frac{\left[1+\frac{4}{\alpha_D}\right]}{\frac{4}{\alpha_D}} \ln\left[e^{-\frac{4}{\alpha_D}\frac{r_D^2}{4t_D}} - (1-k_{\min}/k_{\max})\right] + \frac{4}{\alpha_D}\frac{r_D^2}{4t_D} \right] \text{.(1.6)}$$

"Pressure Derivative in Radial Distance"

$$-r_D \frac{\partial p_D}{\partial r_D} = \left[k_{\min}/k_{\max}\right]^{\frac{\alpha_D}{4}} * \exp\left[-\frac{\left[1+\frac{4}{\alpha_D}\right]}{\frac{4}{\alpha_D}} \ln\left[e^{-\frac{4}{\alpha_D}\frac{r_D^2}{4t_D}} - (1-k_{\min}/k_{\max})\right] + \frac{4}{\alpha_D}\frac{r_D^2}{4t_D} \right] \quad (1.7)$$

The most important issue to consider in evaluating Eqs. 1.5-1.7 is that we have made no limiting assumptions in this development — we have simply used the traditional solution approach based on the Boltzmann transform.

We note that Eq. 1.5 cannot be expressed analytically and *must be evaluated numerically*. In our case we have utilized the software *Mathematica*,[2] which is computationally flexible, as well as capable of generating "near exact" results. Eqs. 1.6 and 1.7 are "closed form" results which are essentially identical in form. We note that comparison of Eqs. 1.6 and 1.7 yield the following identity:

$$2\,t_D \frac{\partial p_D}{\partial t_D} = -r_D \frac{\partial p_D}{\partial r_D} \quad \text{.....(1.8)}$$

As noted in Appendix A, Eq. 1.8 is uniquely valid for this case, as well as the homogeneous reservoir solution (this result is a distinct identity for the case of an infinite-acting reservoir).

The α_D parameter is the dimensionless form of the empirical α-parameter given in Eqs. 1.2 and 1.3. A physical definition or explanation of α cannot be made directly; and, for the purpose of this work, we treat the α-parameter simply as a model parameter — in a similar fashion as permeability, skin factor, etc. We believe that the α-parameter represents the aggregate behavior of the relative permeability functions and the fluid properties (probably both gas and gas condensate).

Using the definitions of the dimensionless variables, we define α_D in terms of α as:

$$\alpha_D = \frac{1}{0.0002637}\phi\mu c_t\,\alpha \quad \text{(conventional oilfield units)} \qquad (1.9)$$

For plotting the pressure derivative functions in both time and space we have defined the following definitions: (which are derived by inspection of Eqs. 1.6 and 1.7)

$$p_{Ddt} = t_D \frac{\partial p_D}{\partial t_D} \qquad (1.10)$$

$$p_{Ddr} = \left| r_D \frac{\partial p_D}{\partial r_D} \right| \qquad (1.11)$$

In **Fig. 1.3** we present a log-log format plot of the $p_D(\varepsilon_D)$ function plotted versus the modified Boltzmann transform variable ($r_D^2/(\alpha_D t_D)$). This plot requires some orientation — for example, we can use this plot to consider the pressure drop as a function of distance for a "snapshot" in time. Data from numerical simulation can be compared to this plot as a mechanism to validate the analytical solution (as we will show in a later section). This plot could also be used to consider data presented in terms of time — however, the "1/t" form given by the modified Boltzmann transform variable does not make **Fig. 1.3** particularly convenient for the analysis/interpretation of pressure-time data. The "1/t" format is rigorous, but the current convention of using time (or t_D) would make this plot less likely to be used in practice.

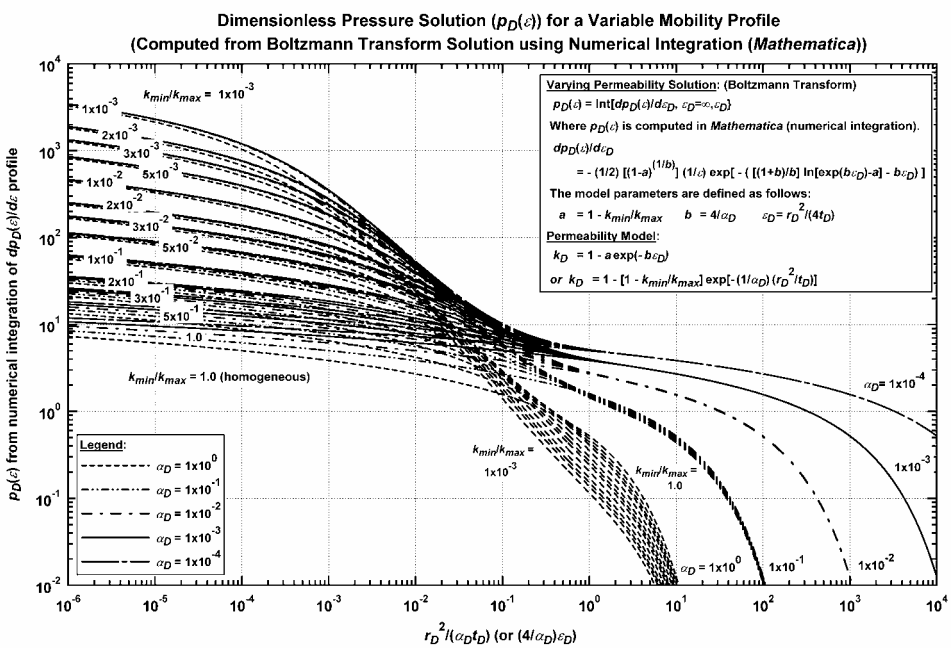

Figure 1.3 – "Type curve" representation of the new model ($p_D(\varepsilon_D)$ formulation (Eq. 1.5)). Solution is plotted versus the modified Boltzmann transform variable ($r_D^2/(\alpha_D t_D)$).

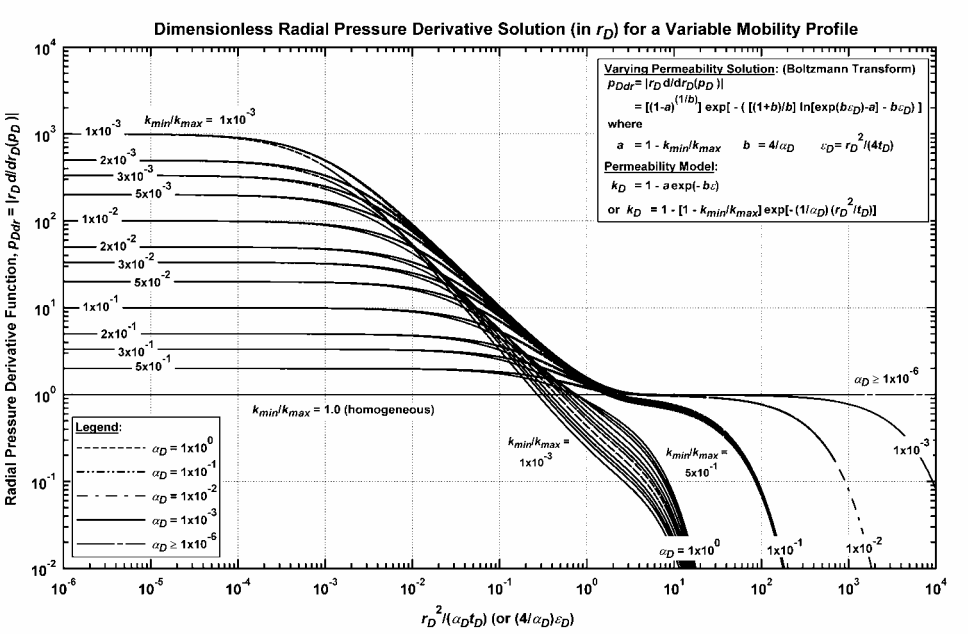

Figure 1.4 – "Type curve" representation of the new model ($|r_D\, dp_D/dr_D|$ formulation (Eq. 1.6)). Solution is plotted versus the modified Boltzmann transform variable ($r_D^2/(\alpha_D t_D)$).

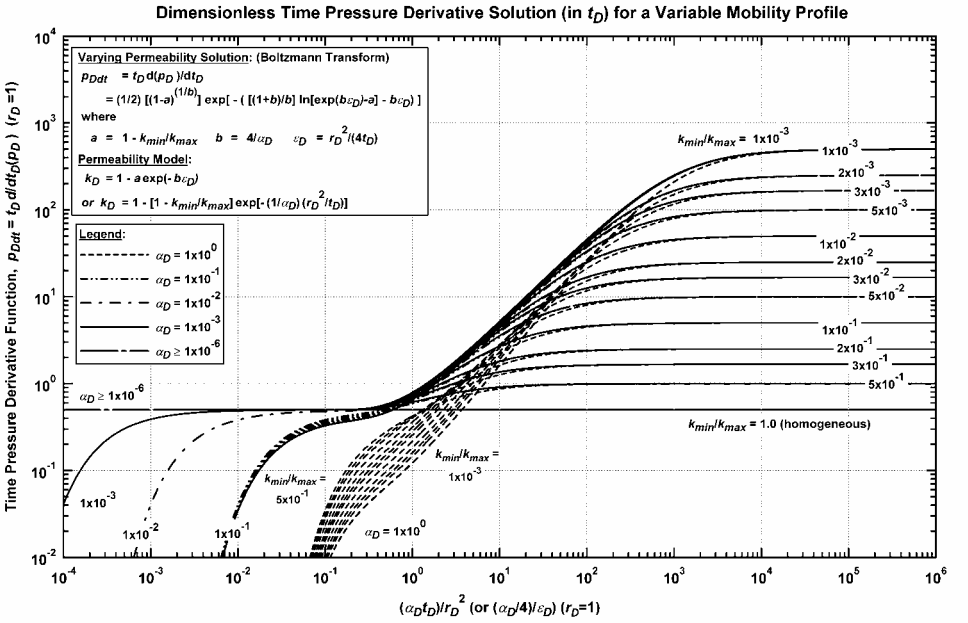

Figure 1.5 – "Type curve" representation of the new model ($t_D(\partial p_D/\partial t_D)$ formulation (Eq. 1.6)). Solution is plotted versus the inverse of the modified Boltzmann transform variable ($(\alpha_D t_D)/r_D^2$).

In **Fig. 1.4** we present the radial derivative function $p_{Ddr}(\varepsilon_D)$ function plotted versus the modified Boltzmann transform variable $(r_D^2/(\alpha_D t_D))$. The $p_{Ddr}(\varepsilon_D)$ formulation represents the change in pressure drop with respect to radius as we move out into the reservoir — clearly there are separate factors at issue — the behavior of the $|r_D(\partial p_D/\partial r_D)|$ (or $|r(\partial p/\partial r)|$) functions show the influence of the propagating permeability profile. In particular, this formulation shows how pressure gradient decreases with distance in the reservoir (as would be expected), but it clearly illustrates the "near well" and "reservoir" behavior of the pressure gradient function. We will utilize **Fig. 1.4** as a "validation plot" for data generated from numeri-cal simulation. In particular, we will match simulated performance to the proposed reservoir model.

Fig. 1.5 presents the time derivative function $p_{Ddt}(\varepsilon_D)$ function (Eq. 1.10) plotted versus the inverse of the modified Boltzmann transform variable $((\alpha_D t_D)/r_D^2)$. In this plot we note that the pressure derivative performance is dramatically influenced by the evolving radial distribution of permeability. It is difficult to make an analogy with this behavior without referencing a particular reservoir model, but the p_{Ddt} performance does appear to represent some sort of flow barrier/impediment at some radial distance. In a later section of this work we will compare the trends shown on **Fig. 1.5** with the responses from several different reservoir models — in particular: the 2-zone radial composite model as well as a sequence of sealing fault models. It is no surprise that these models (*i.e.*, 2-zone radial composite model/sealing fault models) are often used in the interpretation of well test data obtained from gas condensate reservoirs — it is our goal to establish the proposed work as the appropriate standard for the analysis of such data.

1.4 Outline of Thesis

- Chapter I — Introduction
  - Research Problem
  - Research Objectives
  - Summary
- Chapter II — Literature Review
  - Radial Composite Reservoir System
  - General Concepts — $p(r,t)$ Performance in Gas Condensate Reservoirs
  - Other Solutions/Considerations
- Chapter III — Development of an Analytical Pressure Solution for the Case of a Permeability Profile that Varies in Time and Radial Distance
  - Concept of a Mobility Profile that Varies in Time and Radial Distance
  - Application of the Boltzmann Transformation to the Radial Diffusivity Equation — Development of the Pressure Derivative Solutions
  - Wellbore Storage and Skin Effects

- Chapter IV — Validation of an Analytical Pressure Solution for the Case of a Permeability Profile that Varies in Time and Radial Distance — Gas Condensate Reservoirs
  - Comparison of the New Solution and Solutions for the Sealing Faults and Radial Composite Reservoir Cases
  - Validation of the New Solution — Literature Data
- Chapter V — Summary, Conclusions, and Recommendations for Future Work
  - Summary
  - Conclusions
  - Limitations and Recommendations
- Nomenclature
- References
- Appendices
  - Appendix A — Derivation of the Pressure Derivative Functions with Respect to Time and Radius for the Case of a Radially-Varying Permeability Profile (Equivalent Liquid Case)
  - Appendix B — An Approximate Technique for the Direct Addition of Wellbore Storage and Skin Effects
  - Appendix C — A Quadratic Formula for Numerical Differentiation
- Vita

CHAPTER II
LITERATURE REVIEW

2.1 Radial Composite Reservoir System

Historically, much work has been performed in the petroleum industry regarding the study of performance behavior in a reservoir as this performance relates to pressure as a function of time and distance from a vertical well. An accurate understanding of how a reservoir will perform over time in terms of pressure and flowrate is essential for making optimal decisions regarding investment, exploration, and development. In particular, the understanding of gas condensate reservoirs has been very challenging — and study in this area has given the industry insight into this topic, but recent advances in data acquisition and modelling have raised many questions regarding the analysis and interpretation of well performance data obtained from gas condensate reservoirs.

Early work in the petroleum industry focused on the analogy of laminar fluid flow through porous material with the conduction of heat in solids. The behavior of fluids undergoing Darcy (laminar) flow in a radial flow geometry is governed by the radial diffusivity equation (Eq. 1.4). Many solutions of the diffusivity equation for flow in porous materials can be obtained from analog cases in heat conduction (Carslaw and Jaeger[3]), and some cases of "non-uniform" reservoir properties have already been proposed in the heat conduction literature.

In 1970, Ramey[4] presented work which summarized efforts to date for developing practical solutions for fluid flow in 2 and 3-zone radial composite reservoir systems. This work came at a time of intense interest in developing useful and practical solutions for the case of water injection in oil reservoirs (in particular, the development of solutions for injection/falloff tests in such reservoirs). It was Ramey's intent (as implied in his introduction) to derive a class of solutions which contained only elementary functions so that these solutions could be used for the purpose of analysis/interpretation of well test data.

Ramey used the radial diffusivity equation as a starting point, and then added the constraint of two (or more) discrete zones (or "regions") of constant mobility (k/μ) and hydraulic diffusivity ($k/(\phi\mu c)$). This approach gives each discrete region a *constant* permeability, viscosity, porosity, and compressibility — where these properties can vary from region to region. Each region is homogeneous and isotropic, and the change in properties for a particular zone occurs abruptly at the zonal boundary(s). While the physical concept of concentric radial "rings" of differing reservoir properties can be debated, we will note that this solution has been shown to represent a remarkably large number of field cases.

2.2 General Concepts — *p*(*r*,*t*) Performance in Gas Condensate Reservoirs

In 1985, Jones[5] published a Ph.D. dissertation that presented a unified theory for the testing of gas condensate reservoir systems, where this work was based on theory of flow for a slightly compressible liquid as a model for multiphase flow behavior (*i.e.*, the "equivalent liquid" concept). Pseudofunctions (*i.e.*, pseudopressure and pseudotime) were derived for pressure dependent parameters — and in this work Jones developed the "reservoir integral" and "sandface integral" concepts for multiphase flow in porous media. These integrals were adapted from steady-state theory and were the result of reducing the theoretical integrals taken over space and time to integrals taken over pressure. This work provided a definition of pseudopressure that has since shown very good performance in estimating permeability and skin from well tests performed in gas condensate reservoir systems.

In 1989, Bóe, *et al.*[6] proposed a theoretical basis for the analysis of well test data obtained from solution gas and gas condensate reservoir systems during the infinite-acting flow period. Bóe, *et al.* discuss the analysis and interpretation of pressure transient test data using solutions based on the liquid analogy (*i.e.*, the case of a single phase liquid with a small and constant compressibility and constant viscosity). Al-Hussainy, *et. al*[7] suggest that gas tests can be interpreted with this liquid analogy by the use of a pseudopressure function (although as Agarwal[8] (pseudotime) later showed, a pseudotime function is also required for the analysis of pressure buildup tests conducted in gas wells).

Bóe, *et al.* utilize a pseudopressure formulation as well as the Boltzmann transform — where we note that the Boltzmann transform is specifically valid for the infinite-acting period. When the Boltzmann transform is violated by the boundary conditions (*i.e.*, post-transient flow conditions exist), the proposed solution deviates from the liquid analogy (shown in ref. 6). Bóe, *et al.* suggest that as long as infinite-acting flow behavior is observed, the pseudopressure function can be evaluated using the correct pressure/saturation relation at the wellbore. Our work is somewhat comparable in theme to that of Bóe, *et al.* in that we develop a Boltzmann transform solution and then validate the solution using numerical simulation (obviously, the structure of our problem is different, but our approach is similar to that of Bóe, *et al*.).

In 1999, Xu and Lee[9] investigated the condensate gas problem with the intention of improving previous solutions that considered the two-zone, radial composite case. Previous work by Raghavan, Chu, and Jones[10] considered steady-state flow in a two-zone composite model and found that their proposed solutions worked well in cases where the reservoir pressure was substantially higher than dewpoint pressure, and bottomhole flowing pressure in the well was much lower than the dewpoint pressure. However, with the presence of a significant middle zone, where condensate develops, but has not reached critical saturation (*i.e.*, is immobile), the Raghavan, *et al.* solutions are not as accurate. The steady-state flow assumption yields a relationship between condensate saturation in the reservoir and pressure — where this relationship is not valid when flow is impeded by the immobile condensate dropout typically found in Region 2 (*i.e.*, the condensate drop-out zone).

The work by Xu and Lee[9] considers a three-zone radial composite reservoir model. The first zone near the well assumes steady—state two phase flow. The second zone assumes an immobile condensate saturation, but a mobile gas phase. The third zone assumes only dry gas exists in this region. The behavior of these zones is the same as described in the work by Roussennac[1] (where some of Roussennac's comments confirmed the observations put forth by Fevang and Whitson[11]).

For these types of analyses (Fevang and Whitson, Xu and Lee, Roussennac, etc.), relationships had to be developed to represent saturation and pressure for the calculation of the pseudopressure function. The method requires Constant Volume Depletion (CVD) data (for use in modeling Region 2), gas and condensate relative permeability, producing GOR (Region 1), and pressure transient data. Fevang and Whitson[11] proposed the following relationship for Region 1which relates the gas and condensate relative permeability ratio with pressure:

$$\frac{k_{ro}(p)}{k_{rg(p)}} = \frac{1 - r_s R_p}{(R_p - R_s)} \left[\frac{\mu_o B_o}{\mu_g B_g} \right] \quad \text{.....(2.1)}$$

Using pseudopressure functions to approximate the reservoir integral developed by Jones and Raghavan[12] as well as Jones, Vo, and Raghavan[13] ; Xu and Lee[9] compute these pseudopressure functions using the pressure-saturation relationships for Regions 1, 2, and 3 (from whatever source(s) these data may be derived (in most cases numerical simulation)). This procedure (analogous to methods in refs. 7, 14, and 15), allows for the estimation of initial reservoir pressure, formation permeability, and skin factor.

2.3 Other Solutions/Considerations

Wellbore Storage Effects

One of our goals in this work is to generate solutions that can be used for the analysis and interpretation of well test data. In particular, we have chosen to develop "type curve" solutions for the case of wellbore storage effects. Using the liquid analogy, we employed superposition to include the effects of wellbore storage on drawdown solutions (recall that superposition is only valid for the case of linear partial differential equations — where we have presumed that Eq. 1.4 meets these criteria). Blasingame, *et al*[16] provide the derivation and validation of analytical *approximations* for the case of "adding" wellbore storage effects via the Laplace transformation. We have used the methods in ref. 16 to generate the wellbore storage solutions presented in this work (the specific details are presented Appendix B).

For this work we have used "Case 2" presented in ref. 16 (*i.e.*, the case where the $p_{sD}(t_D)$ function is presumed to be linear near a particular time of interest). This result is given by:

$$p_{wD} = \frac{\psi}{\omega}(1 - \exp[-\omega t_D]) + \frac{\theta}{\omega^2}(\exp[-\omega t_D] + \omega t_D - 1) \quad \text{.....(2.2)}$$

The coefficients are ω, ψ and θ are derived using values of the $p_{sD}(t_D)$ function as described in Appendix B. In summary, we are satisfied that the approach given in ref. 16 is robust and sufficiently accurate for our present work — see **Figs. 2.1** and **2.2**, which are validations of Eq. 2.2 prepared in this work for the case of an unfractured well producing in an infinite-acting reservoir.

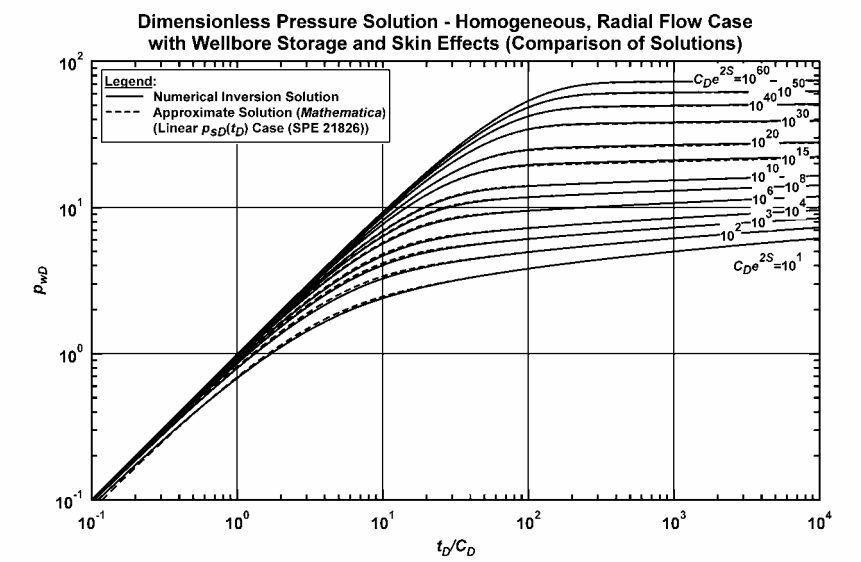

Figure 2.1 – Dimensionless pressure type curve for radial flow behavior including wellbore storage and skin effects (p_{wD} versus t_D/C_D format). This plot presents a comparison of the solution generated using numerical inversion (as a surrogate for the exact solution) and the approximate solution technique proposed in ref. 16 and generated using *Mathematica*.

Pressure Behavior in Time (sealing faults and the 2-zone radial composite solution)

Our new proposed solution for a varying mobility ratio must be compared to existing solutions used for the analysis of pressure transient behavior for gas condensate reservoirs. As such, we consider two cases which are often employed in such analyses — the sealing faults model (various cases) and the 2-zone radial composite reservoir model.

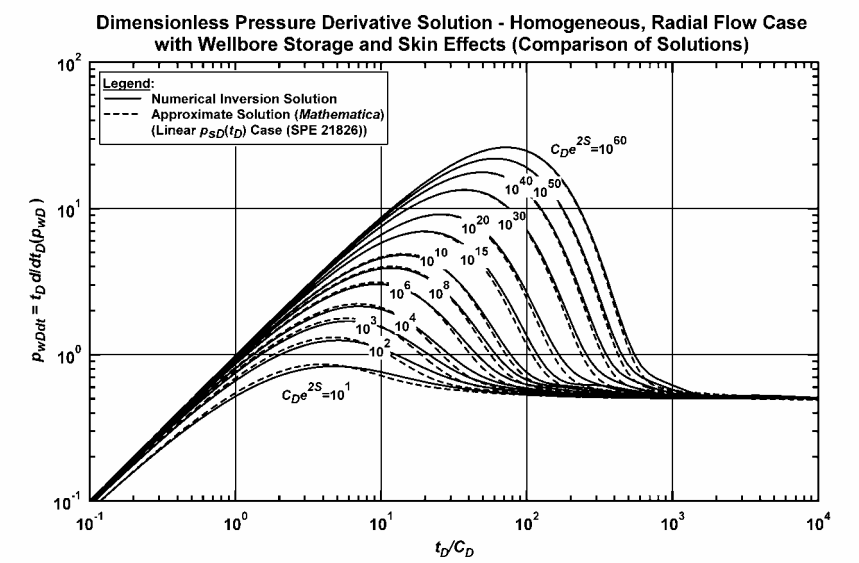

Figure 2.2 – Dimensionless pressure derivative type curve for radial flow behavior including wellbore storage and skin effects (p_{wD}' versus t_D/C_D format). This plot presents a comparison of the solution generated using numerical inversion (as a surrogate for the exact solution) and the approximate solution technique proposed in ref. 16 and generated using *Mathematica*.

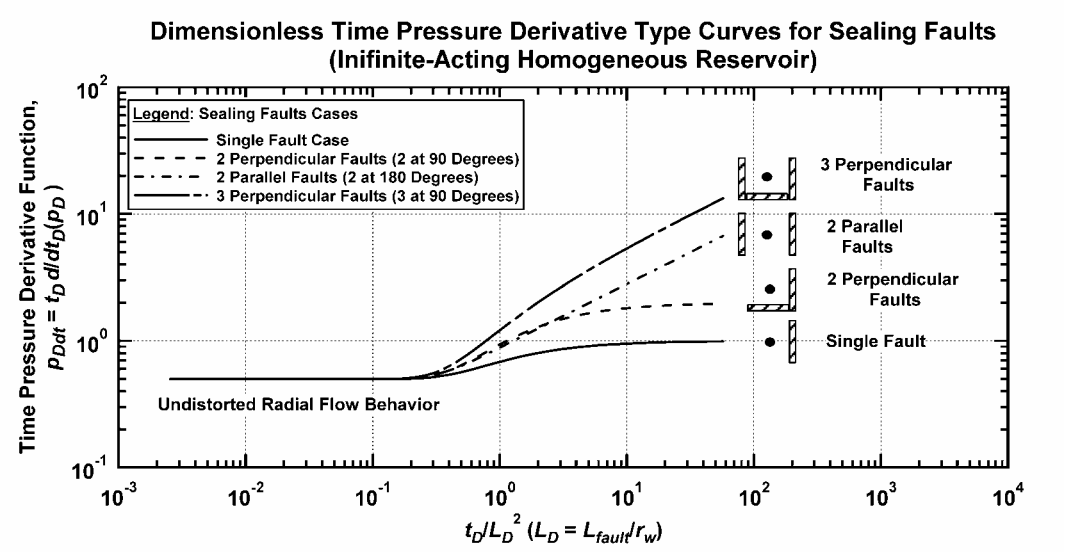

Figure 2.3 – Pressure derivative type curve for a vertical well producing at a constant rate near a sealing fault in a homogeneous, infinite-acting reservoir. (Solution from ref. 14)

The "sealing faults" model is not intuitively applicable for the case of gas condensate reservoir systems — however, the concept of a "flow constriction" or "flow barrier" has been suggested as an analog to the gas condensate case. We do not advocate the use of the "sealing faults" models for the analysis and interpretation of well performance data from gas condensate reservoir systems; we simply note that some analysts have suggested similarity in the performance of the sealing faults models and the observed performance from gas condensate reservoir cases.

In **Fig. 2.3** we present the solution for a well in the vicinity of one or more sealing faults — this presentation clearly indicates that the orientation and number of faults dramatically affects the behavior of the p_{Ddt} function. This solution was obtained from Stewart, *et al.*[14]. In **Fig. 2.4** we present the "unified" plot (p_{Ddt} function) for multiple cases of the radial composite reservoir solution (refs. 15, 17). The most important (and most relevant issue) is that the radial composite solution has fixed mobility and diffusivity ratios (for the inner and outer zones) — by contrast to our solution which uses a permeability profile in radius and time, *but only a single value of diffusivity for the entire reservoir*. As such, we will only compare cases for the radial composite reservoir model where the diffusivity ratio is unity.

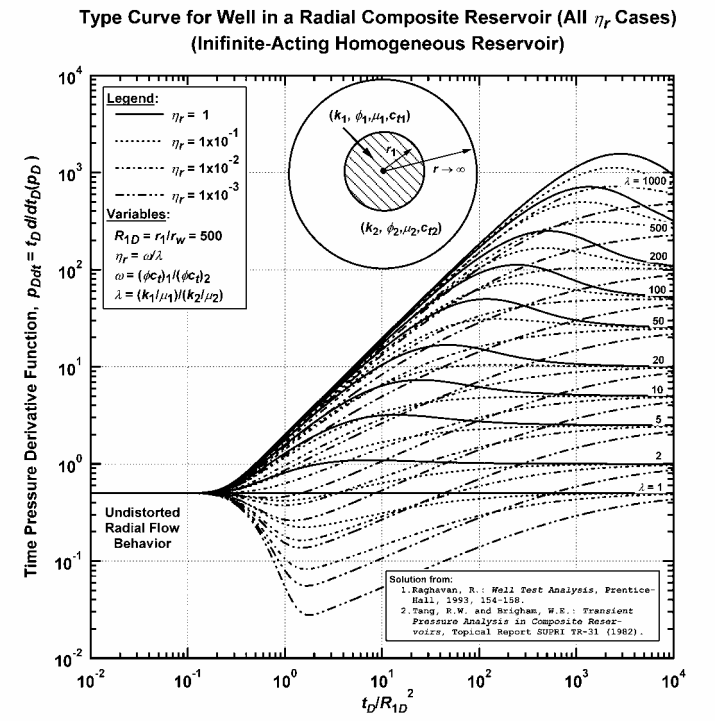

Figure 2.4 – Pressure derivative type curve for a vertical well producing at a constant rate in a composite radial system, various mobility (λ)/storativity (ω) cases. (Solution from refs. 15,17)

CHAPTER III
DEVELOPMENT OF AN ANALYTICAL PRESSURE SOLUTION FOR THE CASE OF A PERMEABILITY PROFILE THAT VARIES IN TIME AND RADIAL DISTANCE

3.1 Concept of a Mobility Profile That Varies in Time and Radial Distance

As noted earlier, we have used the observation of the mobility/effective permeability profiles in radius and time obtained from numerical simulation for the case of a gas condensate reservoir as the basis for our proposed model for gas mobility as a function of radius and time. The original basis for this proposed model was developed using the results published by Roussennac.[1] A sample case adapted from the Roussennac work is shown below in **Fig. 3.1**.

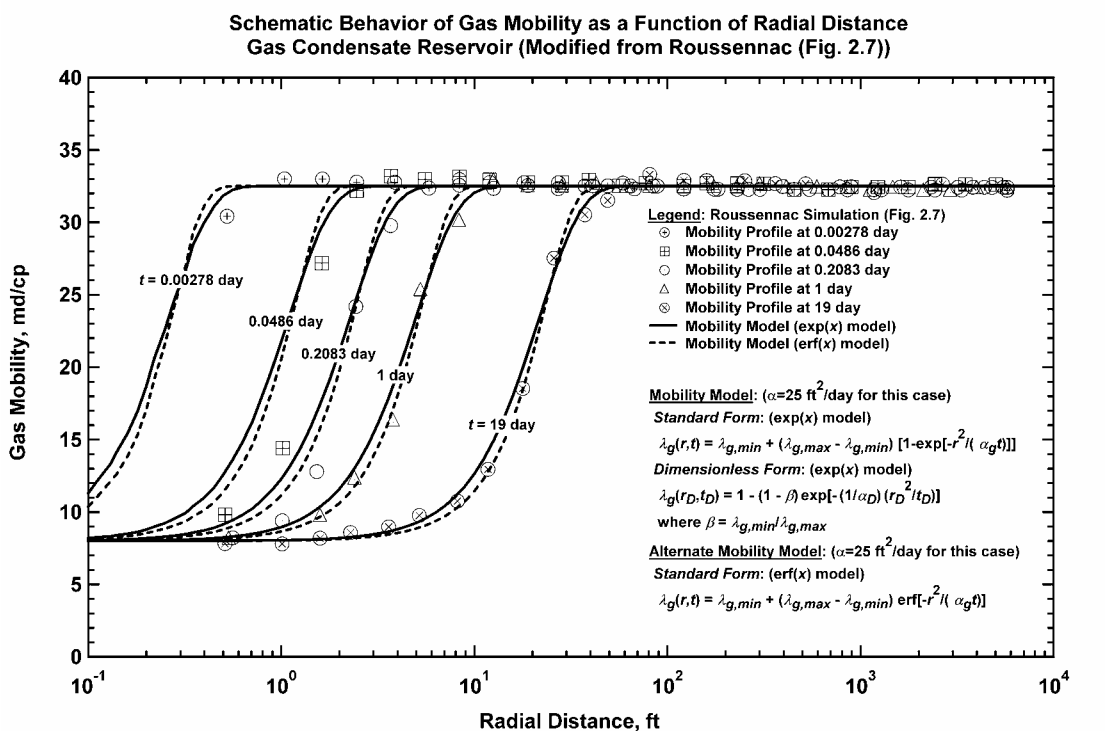

Figure 3.1– Gas mobility profiles for a gas condensate reservoir system (as a function of time and radius) (adapted from Roussennac[1]) — note the comparison of the simulated performance and the proposed models (*i.e.*, the exp(x) and the erf (x) mobility models).

In **Fig. 3.1** we present the following models for representing the gas permeability as a function of radius and pressure — the "exp(x)" model is given as:

$$k = k_{min} + (k_{max} - k_{min}) \left[1 - \exp\left[\frac{-1}{\alpha} \frac{r^2}{t} \right] \right] \quad \text{("exponential" or exp(}x\text{) model)} \quad (3.1)$$

and the "erf(x)" model is given by:

$$k = k_{min} + (k_{max} - k_{min}) \ \text{erf}\left[-\frac{r^2}{\alpha t} \right] \quad \text{("error function" or erf(}x\text{) model)} \quad (3.2)$$

3.2 Application of the Boltzmann Transformation to the Radial Diffusivity Equation — Development of the Pressure Derivative Solutions

In this work we prefer the "exp(x)" model (*i.e.*, Eq. 3.1) — primarily because of the mathematical simplicity of this model (*i.e.*, this model is readily adapted to the Boltzmann transformation approach that is used to develop the solution for this case). As noted in Chapter I, the definition of the diffusivity equation for liquid flow (our base assumption) is given by:

$$\frac{1}{r} \frac{\partial}{\partial r} \left[k\, r \frac{\partial p}{\partial r} \right] = \frac{1}{0.0002637} \phi \mu c_t \frac{\partial p}{\partial t} \quad \text{(Field units)} \quad (3.3)$$

Assuming that the permeability is a function of radius and time $k=f(r,t)$, we obtain the following generalized dimensionless form of the diffusivity equation based on the Boltzmann transformation (details in Appendix A):

$$\frac{d^2 p_D}{d\varepsilon_D^2} + \left[\frac{1}{\varepsilon_D} + \frac{1}{k_D} \left[1 + \frac{dk_D}{d\varepsilon_D} \right] \right] \frac{dp_D}{d\varepsilon_D} = 0 \quad (3.4)$$

Given Eq. 3.4 in dimensionless form we note the definitions of the relevant dimensionless variables:

$$\varepsilon_D = r_D^2 / 4t_D \quad \text{(dimensionless Boltzmann transform parameter)} \quad (3.5)$$

$$k_D = k/k_{max} \quad \text{(dimensionless permeability (note in terms of } k_{max}\text{))} \quad (3.6)$$

$$p_D = \frac{1}{141.2} \frac{k_{max} h}{qB\mu} (p_i - p) \quad \text{(dimensionless pressure)} \quad (3.7)$$

$$t_D = 0.0002637 \frac{k_{max}}{\phi \mu c_t r_w^2} t \quad \text{(dimensionless time)} \quad (3.8)$$

$$r_D = r/r_w \quad \text{(dimensionless radius)} \quad (3.9)$$

Using these definitions, the dimensionless form of the permeability function (*i.e.*, Eq., 3.1) is given by:

$$k_D = 1 - \left[1 - \frac{k_{\min}}{k_{\max}} \right] \exp\left[\frac{-4}{\alpha_D} \varepsilon_D \right] \quad (3.10)$$

For convenience, we define the constants a and b as follows:

$$a = (1 - k_{min}/k_{max}) \quad (3.11)$$

$$b = 4/\alpha_D \quad (3.12)$$

Substituting Eqs. 3.11 and 3.12 into Eq. 3.10 yields:

$$k_D = 1 - a\,exp[-b\varepsilon_D] \quad \text{..... (3.13)}$$

Substituting Eq. 3.13 into Eq. 3.4 and completing the solution (using the Boltzmann transformation process), we obtain the following solutions: (again, the details of this derivation are given in Appendix A)

$$\varepsilon_D \frac{dp_D}{d\varepsilon_D} = -\frac{1}{2}(k_{min}/k_{max})^{\frac{\alpha_D}{4}} \exp\left[-\frac{(1+\frac{4}{\alpha_D})}{\frac{4}{\alpha_D}} \ln\left[e^{-\frac{4}{\alpha_D}\varepsilon_D} - (1-k_{min}/k_{max}) \right] + \frac{4}{\alpha_D}\varepsilon_D \right]$$

("derivative" form) ..... (3.14)

$$p_D(\varepsilon_D) = \frac{1}{2}(k_{min}/k_{max})^{\frac{\alpha_D}{4}} \int_{\varepsilon_D}^{\infty} \left[\frac{1}{\varepsilon_D} \exp\left[-\frac{(1+\frac{4}{\alpha_D})}{\frac{4}{\alpha_D}} \ln\left[e^{-\frac{4}{\alpha_D}\varepsilon_D} - (1-k_{min}/k_{max}) \right] + \frac{4}{\alpha_D}\varepsilon_D \right] \right] d\varepsilon_D$$

("pressure" form) ..... (3.15)

Alternate forms of Eq. 3.14, written in terms of r_D and t_D are given as:.

$$-r_D \frac{\partial p_D}{\partial r_D} = (k_{min}/k_{max})^{\frac{\alpha_D}{4}} \exp\left[-\frac{(1+\frac{4}{\alpha_D})}{\frac{4}{\alpha_D}} \ln\left[e^{-\frac{4}{\alpha_D}\varepsilon_D} - (1-k_{min}/k_{max}) \right] + \frac{4}{\alpha_D}\frac{r_D^2}{4t_D} \right]$$

("r_D derivative" form) ..... (3.16)

$$t_D \frac{\partial p_D}{\partial t_D} = \frac{1}{2}(k_{min}/k_{max})^{\frac{\alpha_D}{4}} \exp\left[-\frac{(1+\frac{4}{\alpha_D})}{\frac{4}{\alpha_D}} \ln\left[e^{-\frac{4}{\alpha_D}\varepsilon_D} - (1-k_{min}/k_{max}) \right] + \frac{4}{\alpha_D}\frac{r_D^2}{4t_D} \right]$$

("t_D derivative" form) ..... (3.17)

Inspection of Eq. 3.12 (the "pressure" form of the solution) leads us to recognize that Eq. 3.12 can not be resolved as a closed form solution — this result can only be evaluated numerically. As such, we have elected to use Mathematica[2] to compute the p_D and $|\varepsilon_D\ dp_D/d\varepsilon_D|$ solutions. We present a variety of solutions for the p_D and $|\varepsilon_D\ dp_D/d\varepsilon_D|$ functions in **Figs. 3.2** and **3.3** — where the p_D function is shown in **Fig. 3.2** and the $|\varepsilon_D\ dp_D/d\varepsilon_D|$ function is presented in **Figs. 3.3.**

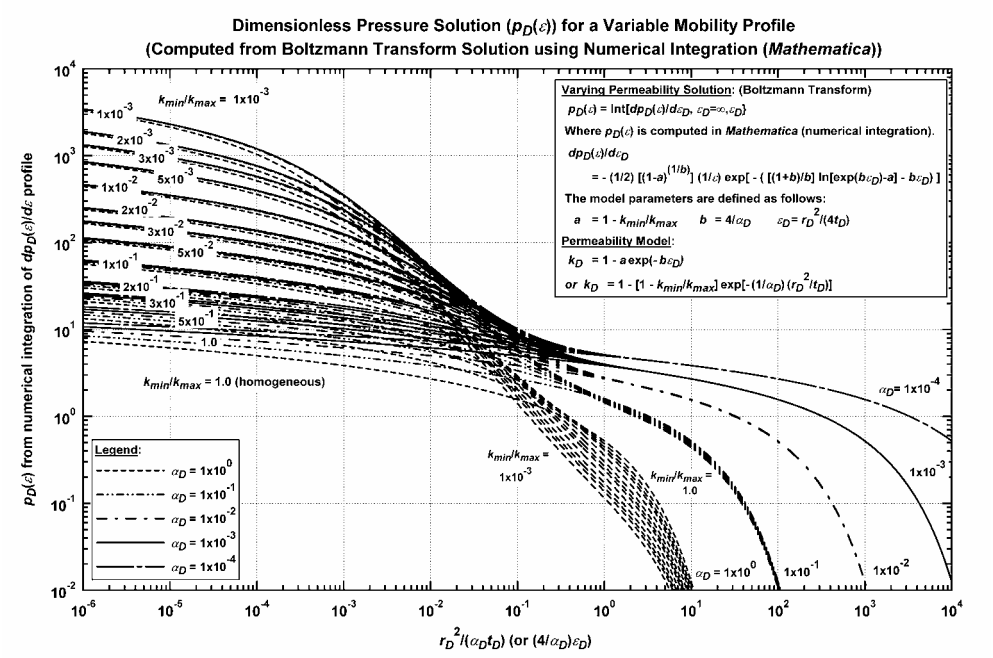

Figure 3.2 – "Type curve" representation of the $p_D(\varepsilon_D)$ solution (Eq. 3.12)). Solution is plotted versus the modified Boltzmann transform variable ($r_D^2/(\alpha_D t_D)$).

In **Fig. 3.2** we can view these trends as being the pressure drop (in dimensionless form) taken as distance increases away from the wellbore as we hold time constant. We note the effect of the k_{min}/k_{max} ratio on the performance of the p_D solution — and we observe that the α_D-parameter is as a scaling mechanism in the modified Boltzmann transform variable ($r_D^2/(\alpha_D t_D)$). We would describe this situation physically as a decreasing pressure drop as we progress into the reservoir, noting that the k_{min}/k_{max} ratio controls the pressure drop near the well — and that the combination of the k_{min}/k_{max} ratio and the α_D-parameter control the transition and "far field" pressure solutions.

Fig. 3.3 presents the $dp_D/d\varepsilon_D$ solution for the same k_{min}/k_{max} and α_D cases shown in **Fig. 3.2**. In this case we note the distinct similarity of the $|\varepsilon_D\, dp_D/d\varepsilon_D|$ solution with the $|r_D\, dp_D/dr_D|$ solution (Fig. 1.5) — this is because these functions are simply "rescaled" (*i.e.*, $|r_D\, dp_D/dr_D| = 2\ |\varepsilon_D\, dp_D/d\varepsilon_D|$ (comparing Eq. 1.7 with Eq. 3.11)). **Fig. 3.3** is of relatively little practical utility unless we work in terms of the variable $\eta=r^2/t$ (we note that we do present several comparisons in terms of η, but for practical applications solutions in t (time) are of more direct use).

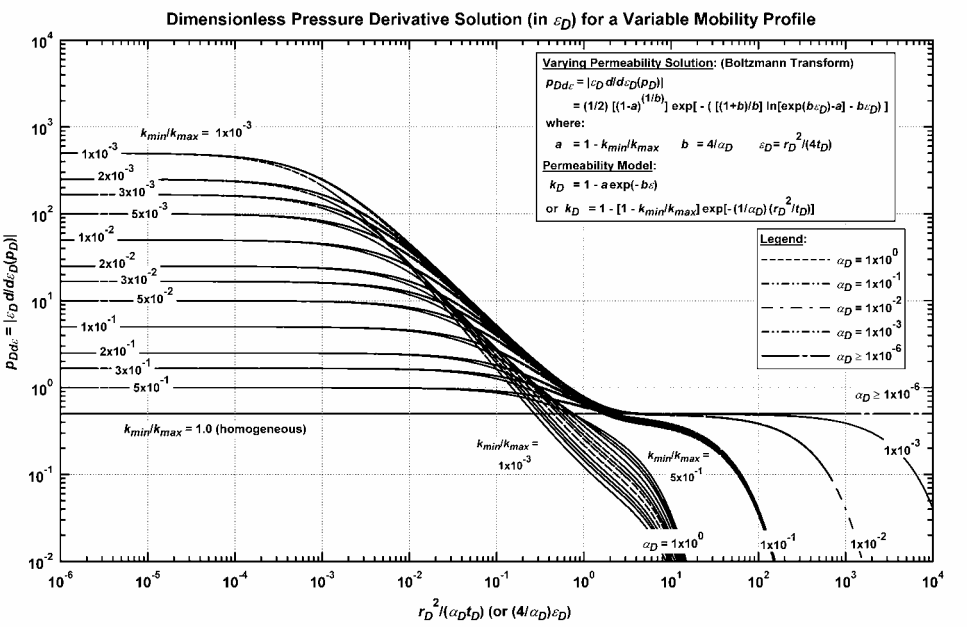

Figure 3.3 – "Type curve" representation of the $|\varepsilon_D\, dp_D/d\varepsilon_D|$ solution (Eq. 3.11)). Solution is plotted versus the modified Boltzmann transform variable ($r_D^2/(\alpha_D t_D)$).

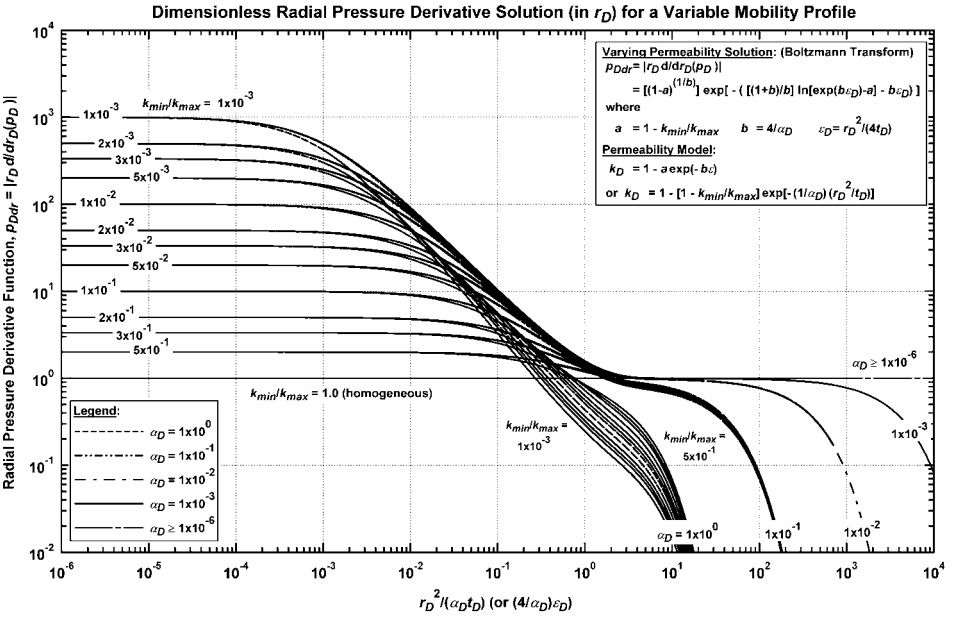

Figure 3.4 – "Type curve" representation of the new model ($|r_D\, dp_D/dr_D|$ formulation (Eq. 1.6)). Solution is plotted versus the modified Boltzmann transform variable ($r_D^2/(\alpha_D t_D)$).

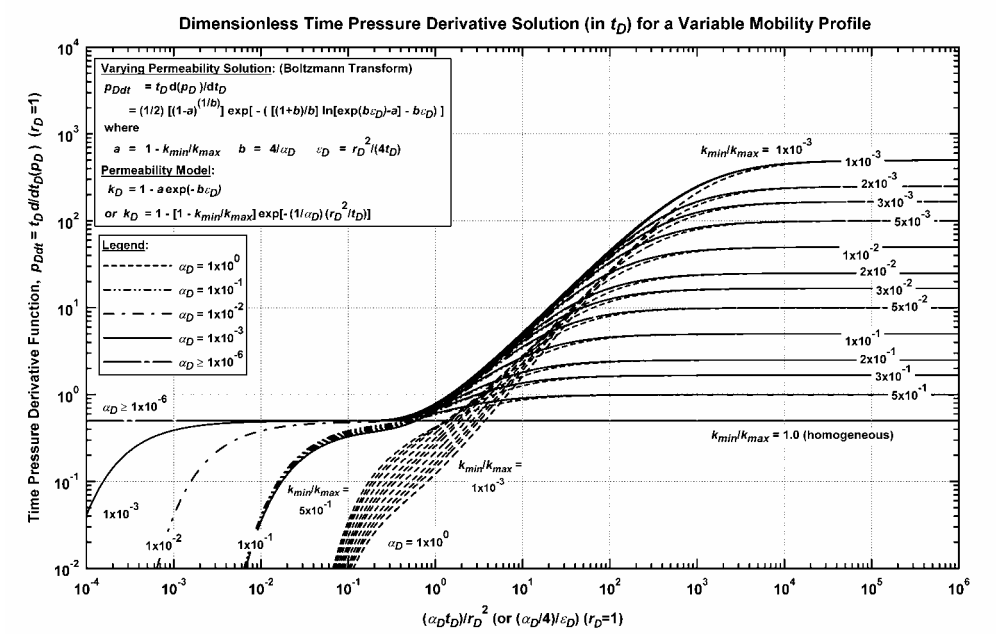

Figure 3.5 – "Type curve" representation of the new model ($t_D(\partial p_D/\partial t_D)$ formulation (Eq. 1.6)). Solution is plotted versus the inverse of the modified Boltzmann transform variable ($(\alpha_D t_D)/r_D^2$).

We also present the pressure derivative solutions plotted in terms of variables related to dimensionless radius and time in **Figs. 3.4** and **3.5** (we continue to use a modification of the dimensionless Boltzmann transform variable). **Fig. 3.4** (the radius format plot) will be used to validate simulated performance data where we will have pressure values at a specific spatial grid as generated by numerical simulation.

We could use **Fig. 3.5** as an analysis mechanism for pressure transient data — however, as we discuss in the next section, for practical applications, the solution must be modified to include wellbore storage effects. **Fig. 3.5** will also be used in the validation portion of this work to compare against the existing solutions which are often utilized in the analysis of pressure transient test data obtained from gas condensate reservoir systems (namely, the 2-zone radial composite reservoir case and the "sealing faults" cases).

3.3 Wellbore Storage and Skin Effects

Addition of Wellbore Storage Effects — Drawdown Cases (*Base Comparisons*)

So far in this work we have only considered the case of an ideal well producing in an infinite-acting reservoir with a propagating permeability profile — where the well is produced at a single-constant flowrate. In this section we provide a mechanism for adding wellbore storage effects to our new solution for a propagating permeability profile. Wellbore storage is typically "added" to the base pressure solution using convolution (or superposition) — where we believe that convolution should be valid for this problem

because we have assumed that are no non-linearities in the governing differential equation (Eq. 4). As such, the convolution for wellbore storage is written as:

$$p_{wD} = \int_0^{t_D} \frac{d}{d\tau}\left[q_{Dwbs}(\tau)\right] p_{sD}(t_D - \tau)\, dt_D \quad \text{.....(3.18)}$$

Where the q_D function (dimensionless sandface rate profile) is given as follows for the wellbore storage model:

$$q_{Dwbs} = \frac{q_{sf}}{q_{sur}} = 1 - C_D \frac{d}{dt_D}\left[p_{wD}\right] \quad \text{.....(3.19)}$$

And the definition of the dimensionless pressure function which includes skin effects is given as:

$$p_{sD} = p_D + s \quad \text{.....(3.20)}$$

Eqs. 3.18 and 3.19 can be discretized and combined to yield a "recursion relation" for the wellbore storage dimensionless pressure, p_{wD} — however, this approach is tedious and prone to error propagation. Typical implementations of Eqs. 3.18 and 3.19 involve the use of the Laplace transformation — unfortunately, our proposed solution (Eq. 3.14) is not suited to the use of the Laplace transform (*i.e.*, this solution can not be integrated analytically), and, as such, we must resort to another approach.

For convenience we employ the method by Blasingame, *et al.*[16] for generating pressure solutions which include wellbore storage and skin effects — the solution used in this work is given in Appendix B.

We provide **Figs. 3.6a and 3.6b** as validations for the Blasingame, *et al.* method — specifically for the case of well producing in an infinite-acting homogeneous reservoir. The p_{wDt} function is computed using the procedures given in Appendix B and the p_{wDdt} function is computed using the procedures given in

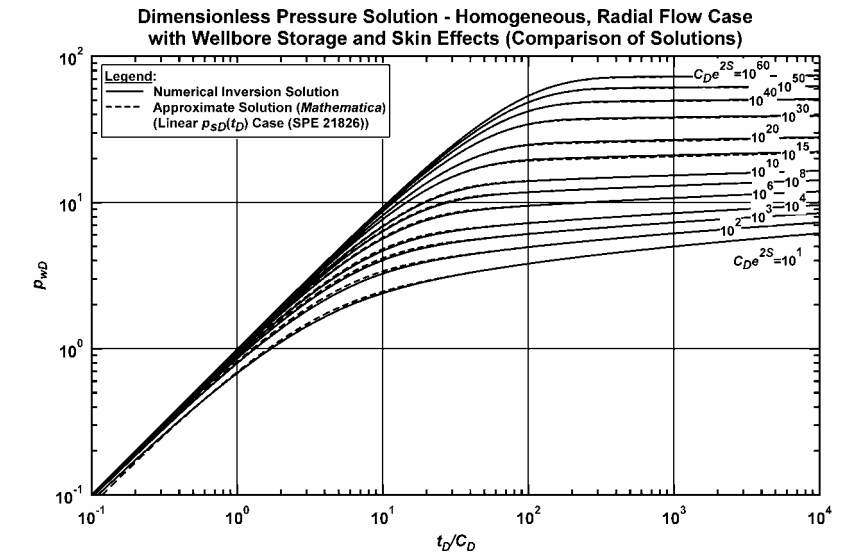

Figure 3.6a– Dimensionless pressure type curve for radial flow behavior including wellbore storage and skin effects (p_{wD} versus t_D/C_D format). This plot presents a comparison of the solution generated using numerical inversion (as a surrogate for the exact solution) and the approximate solution technique proposed in ref. 16 and generated using *Mathematica*.

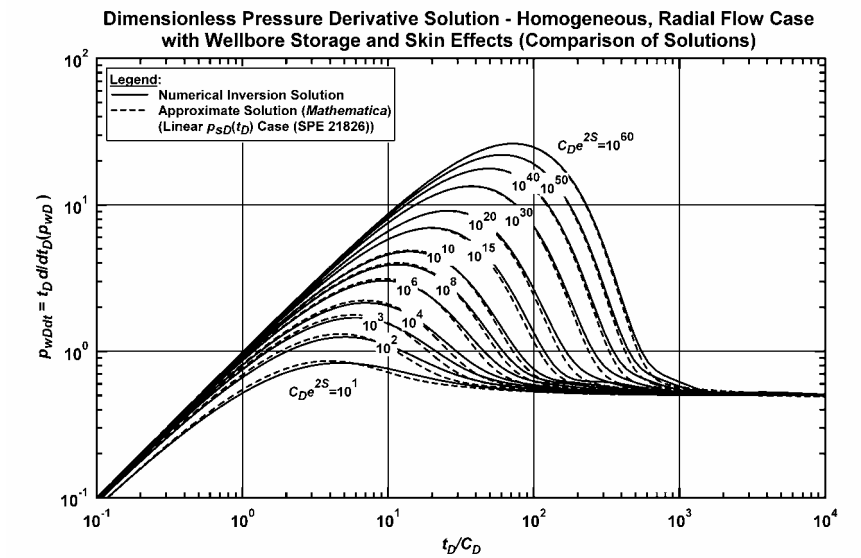

Figure 3.6b– Dimensionless pressure derivative type curve for radial flow behavior including wellbore storage and skin effects (p_{wD}' versus t_D/C_D format). This plot presents a comparison of the solution generated using numerical inversion (as a surrogate for the exact solution) and the approximate solution technique proposed in ref. 16 and generated using *Mathematica*.

Appendix C (we note that we have used a polynomial regression (a 3-point formula) to calculate the p_{wDdt} function). Excellent agreement exists between the "exact" solutions (*i.e.*, the numerical inversion solution) and the approximate solutions provided by the methods given in ref. 16. By extension, we will apply the procedures given in Appendices B and C to our new solution for a radially propagating permeability function.

In **Figs. 3.7a-3.7f** we provide a sequence of solutions for the specific case of C_D=1x10^3 and for cases where the k_{min}/k_{max} varies from 1x10^0 to 1x10^{-3}. Individual plots consider a single value of the α_D-parameter, and the following cases of α_D=1x10^0, 10^{-1}, 10^{-2}, 10^{-3}, 10^{-4}, 10^{-5} are considered (**Figs. 3.7a-3.7f**, respectively). **Figs. 3.7a-3.7f** illustrate the "evolving" effects of the α_D-parameter, and we note that non-unique effects are possible (*i.e.*, a particular case or trend which appears similar to another case, although these cases have substantially different base properties (*e.g.*, k_{min}/k_{max}, α_D, etc.)). Most of the cases in **Figs. 3.7a-3.7f** should be described as unique (although **Figs. 3.7b and 3.7c** do appear to be very similar).

Addition of Wellbore Storage Effects — Drawdown Cases (*t_D/C_D Format Plots*)

Another objective for work in this section is to establish the general character/behavior of such results. In **Fig. 3.8** we present a "composite" plot of all p_{wDdt} trends generated for C_D=1x10^3. We note distinct behavior for each case and we suggest that the character in these wellbore storage solutions (for this particular case) is both accurate and distinct. Similarly, in **Fig. 3.9** we present the same suite of solutions for C_D=1x10^{20}. The most obvious comment we can make is that virtually all of the trends generated for the C_D=1x10^{20} case are dominated by wellbore storage effects — *i.e.*, the α_D-parameter has virtually no influence on the response of the solution for the C_D=1x10^{20} case.

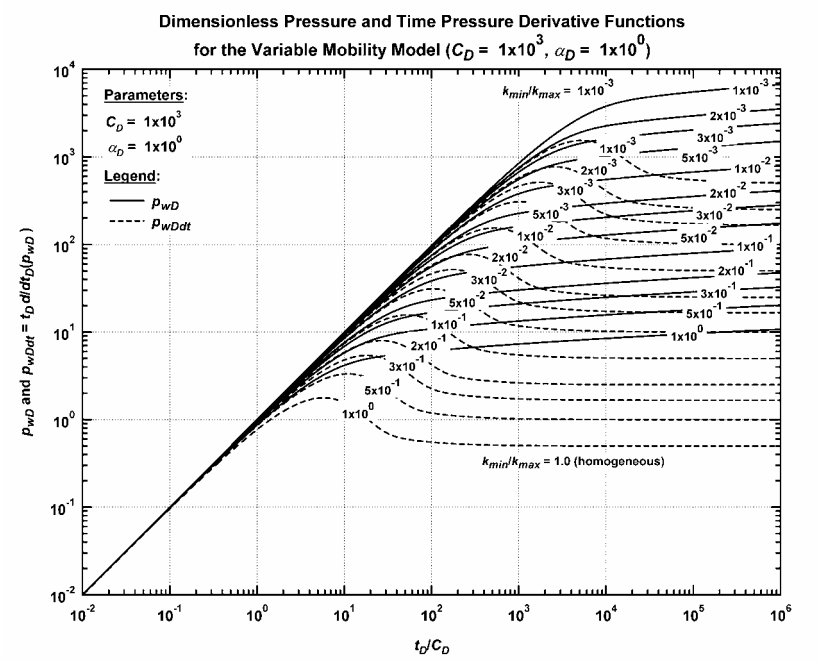

Figure 3.7a– Type curve plot (p_{wD} and p_{wD}' versus t_D/C_D) — $C_D = 1\text{x}10^3$, $\alpha_D = 1\text{x}10^0$, various k_{min}/k_{max} cases.

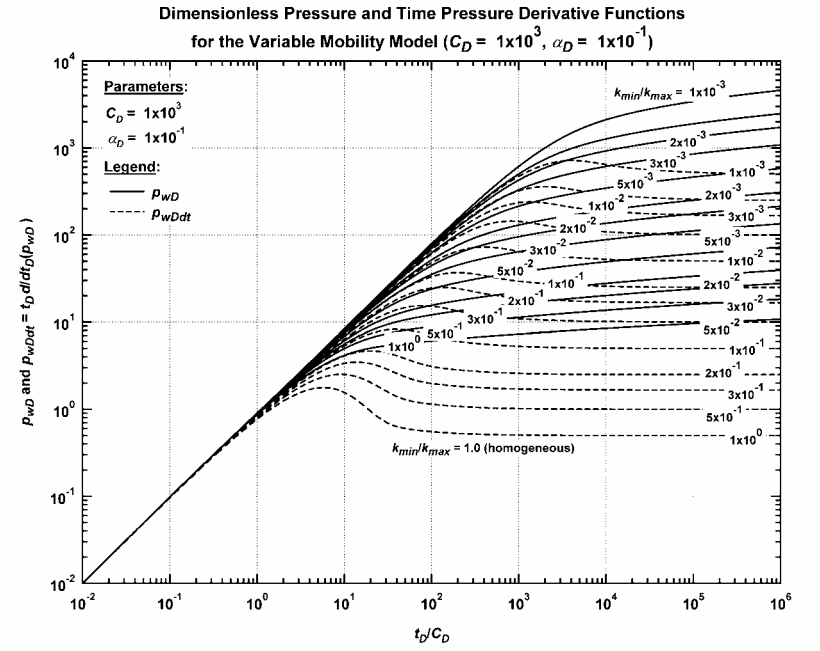

Figure 3.7b– Type curve plot (p_{wD} and p_{wD}' versus t_D/C_D) — $C_D = 1\text{x}10^3$, $\alpha_D = 1\text{x}10^{-1}$, various k_{min}/k_{max} cases.

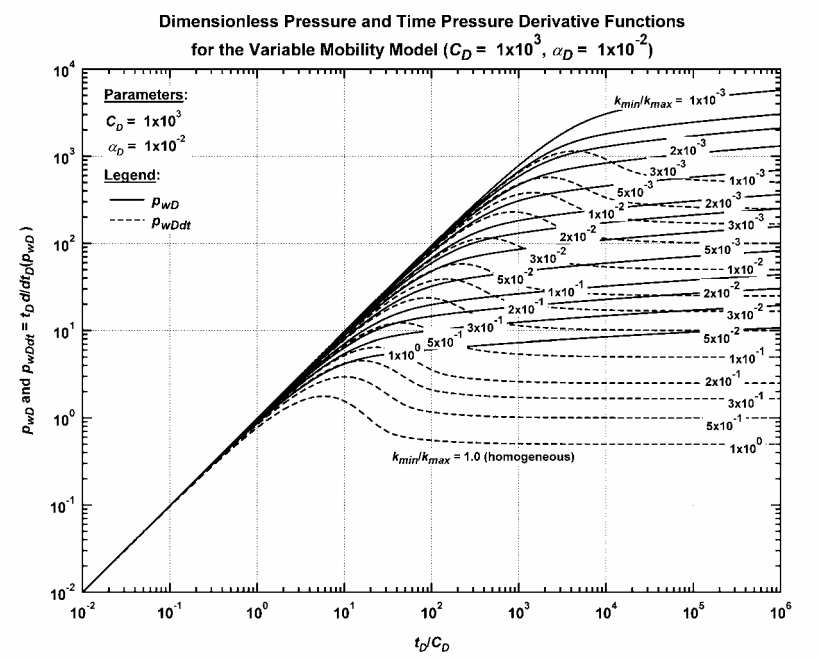

Figure 3.7c– Type curve plot (p_{wD} and p_{wD}' versus t_D/C_D) — $C_D = 1\text{x}10^3$, $\alpha_D = 1\text{x}10^{-2}$, various k_{min}/k_{max} cases.

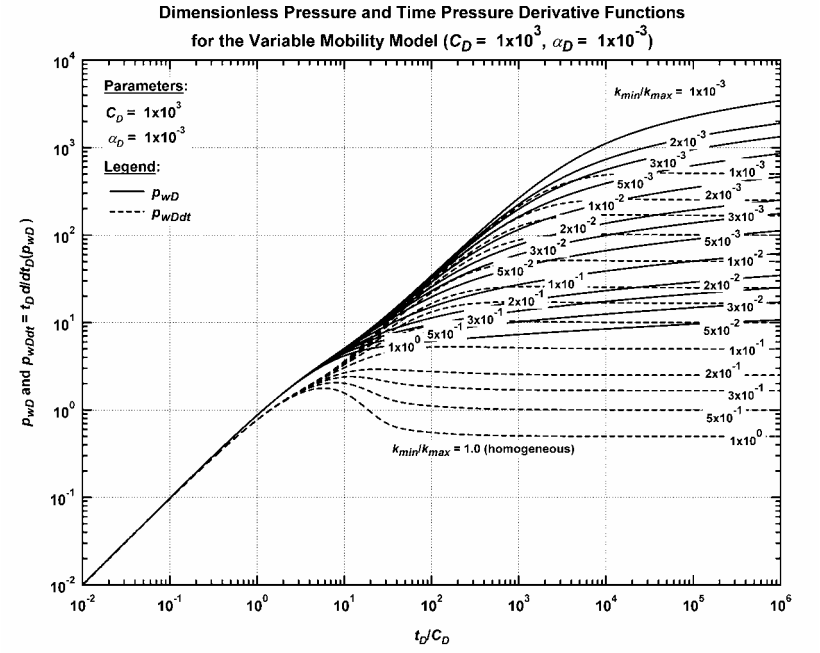

Figure 3.7d– Type curve plot (p_{wD} and p_{wD}' versus t_D/C_D) — $C_D = 1\text{x}10^3$, $\alpha_D = 1\text{x}10^{-3}$, various k_{min}/k_{max} cases.

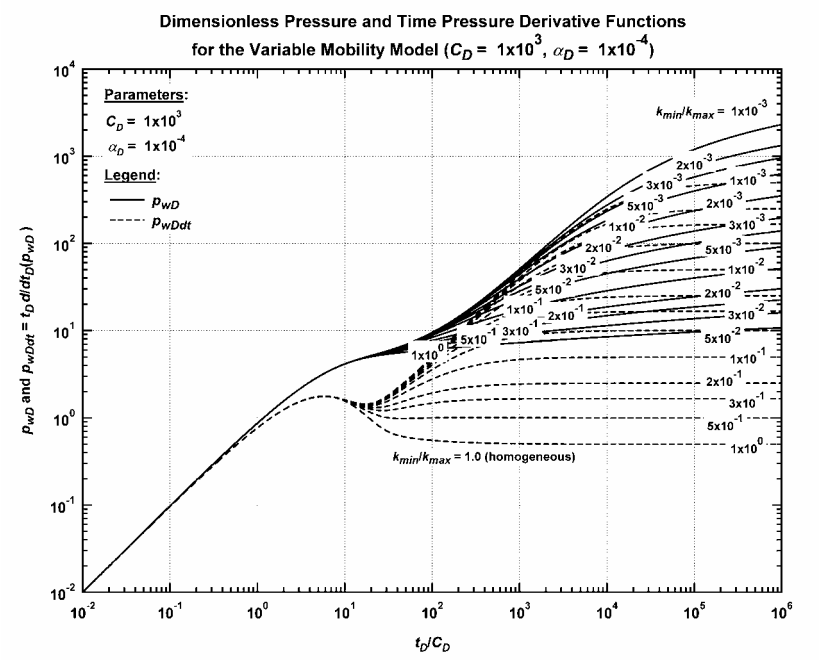

Figure 3.7e – Type curve plot (p_{wD} and p_{wD}' versus t_D/C_D) — C_D = 1x10^3, α_D = 1x10^{-4}, various k_{min}/k_{max} cases.

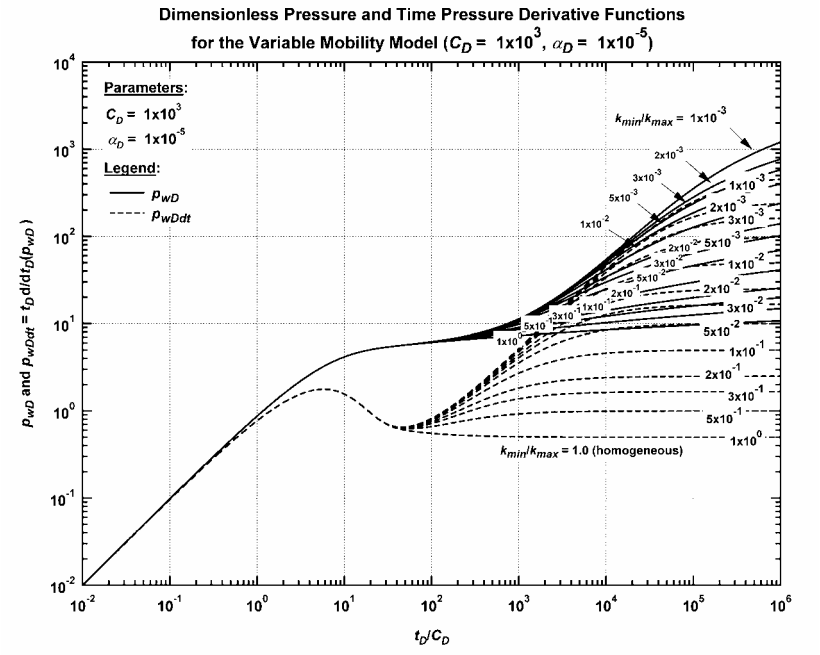

Figure 3.7f – Type curve plot (p_{wD} and p_{wD}' versus t_D/C_D) — C_D = 1x10^3, α_D = 1x10^{-5}, various k_{min}/k_{max} cases.

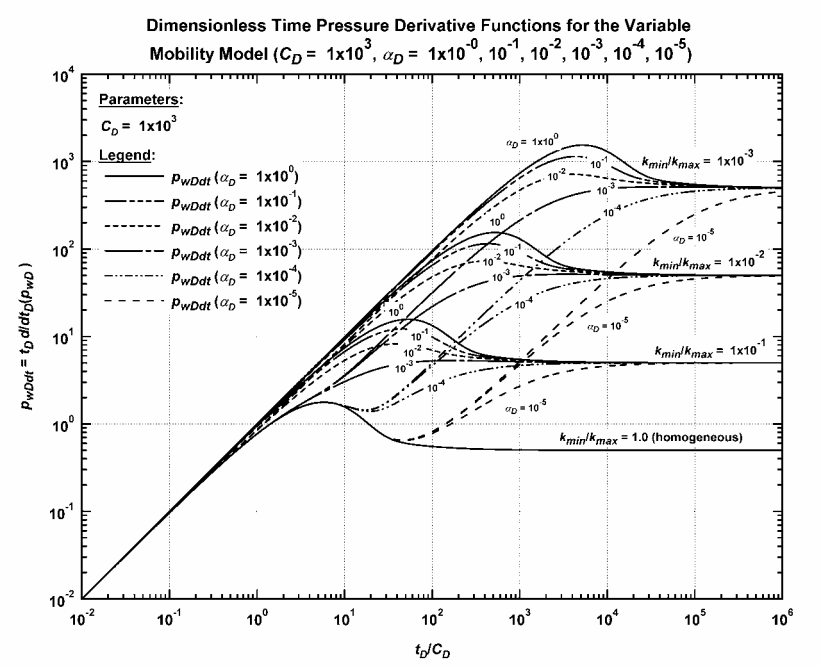

Figure 3.8 – Drawdown type curve plot (p_{wD}' versus t_D/C_D) — C_D = 1x10^3, α_D = 1x10^0, 10^{-1}, 10^{-2}, 10^{-3}, 10^{-4}, 10$^{-5,}$ various k_{min}/k_{max} = 1x10^0, 10^{-1}, 10^{-2}, 10^{-3}.

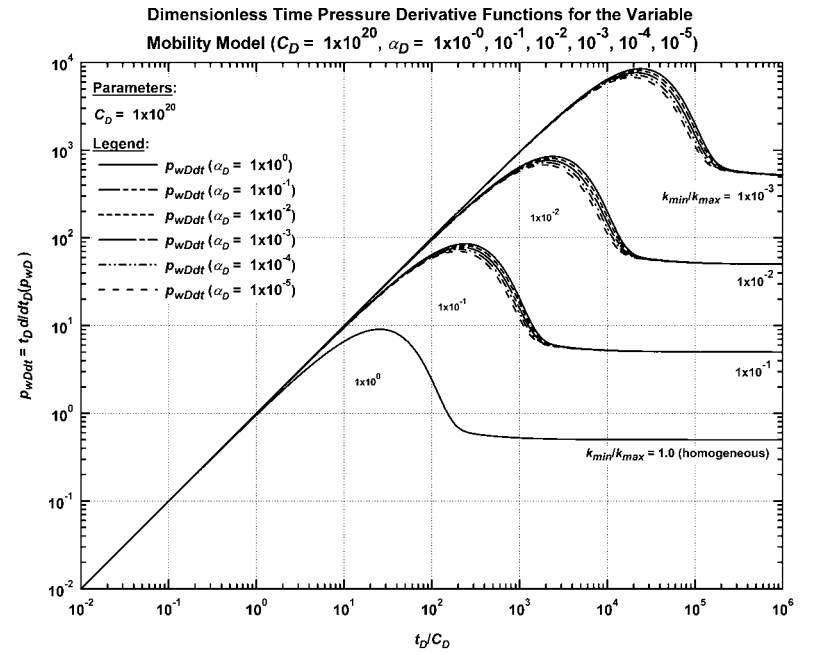

Figure 3.9 – Drawdown type curve plot (p_{wD}' versus t_D/C_D) — C_D = 1x10^{20}, α_D = 1x10^0, 10^{-1}, 10^{-2}, 10^{-3}, 10^{-4}, 10$^{-5,}$ various k_{min}/k_{max} = 1x10^0, 10^{-1}, 10^{-2}, 10^{-3}.

CHAPTER IV
VALIDATION OF AN ANALYTICAL PRESSURE SOLUTION FOR THE CASE OF A PERMEABILITY PROFILE THAT VARIES IN TIME AND RADIAL DISTANCE — GAS CONDENSATE RESERVOIRS

4.1 Comparison of the New Solution and Solutions for the Sealing Faults and Radial Composite Reservoir Cases

Pressure Behavior in Time

Our goal is to provide a qualitative comparison of the new proposed solution (the result given in terms of time) and the 2-zone radial composite reservoir model — where we note that the radial composite model is the most commonly used reservoir model for the interpretation and analysis of well test data from gas condensate reservoirs. We also present a comparison of the proposed model with the model for a well in the vicinity of one or more "sealing faults" — where our goal is to simply compare the influence of our new model as a "flow constriction" or "flow barrier." We are not advocating the use of the "sealing faults" models for the analysis and interpretation of well performance data in gas condensate reservoir systems; we are simply making a qualitative (graphical) comparison of the solutions.

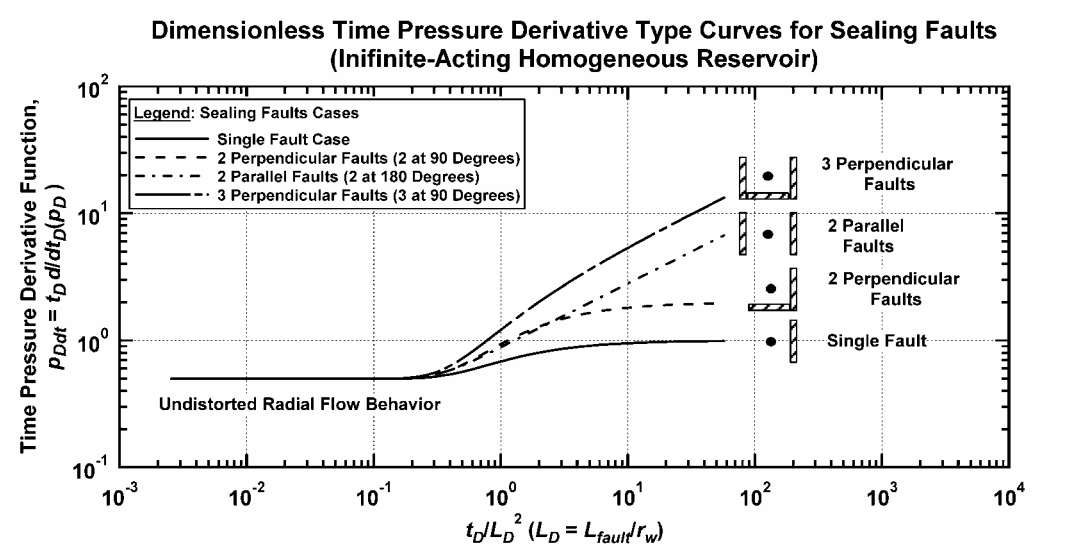

Figure 4.1 – Pressure derivative type curve for a vertical well producing at a constant rate near a sealing fault in a homogeneous, infinite-acting reservoir.

In **Fig. 4.1** we present the solution for a well in the vicinity of one or more sealing faults — this presentation clearly indicates that the orientation and number of faults dramatically affects the behavior of the p_{Ddt} function. In **Fig. 4.2** we present the "unified" plot (p_{Ddt} function) for multiple cases of the radial composite reservoir solution. The most important, and most relevant issue is that the radial composite solution has fixed mobility and diffusivity ratios (for the inner and outer zones). This use of fixed mobility and diffusivity ratios is in direct contrast to our solution which uses a permeability profile in radius and time, *but only a single value of diffusivity for the entire reservoir*. As such, we will only compare cases for the radial composite reservoir model where the diffusivity ratio is unity.

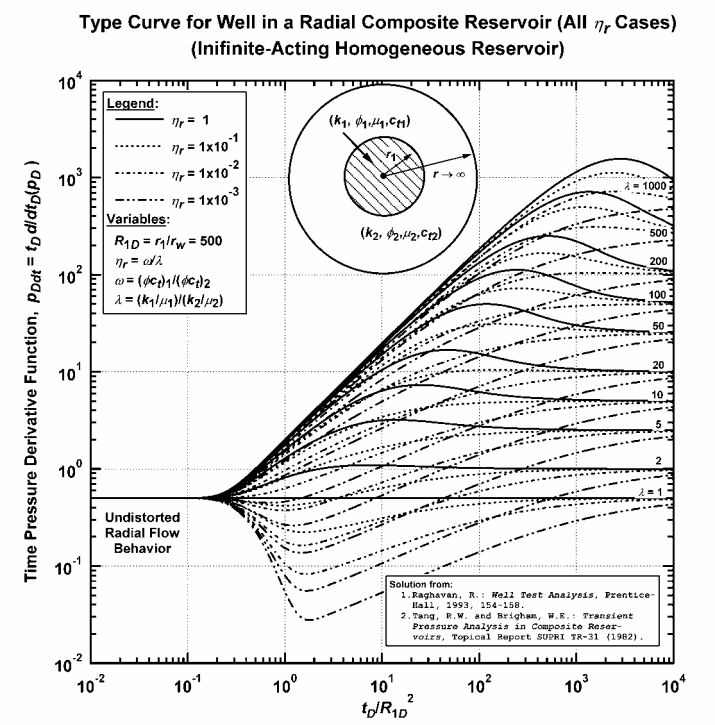

Figure 4.2 – Pressure derivative type curve for a vertical well producing at a constant flowrate in a 2-zone radial composite reservoir system, various mobility (λ)/storativity (ω) cases.

In **Fig. 4.3** we present a combined plot of all three reservoir cases: the sealing faults case, the 2-zone radial composite reservoir case, and our proposed reservoir model for a permeability profile which varies in time and radial distance. We note surprising similarity for the results shown in **Fig. 4.3** — despite the fact that the reservoir models shown have little in common. One interpretation could be that this behavior is a cause for concern since the models are distinctly different — yet produce similar behavior. Another interpretation could be that the 2-zone (fixed) radial composite reservoir model and the new propagating

permeability profile model have, at least in concept, a common denominator of 2 dominant permeabilities (*i.e.*, the "near well" and "reservoir" permeabilities).

In fact, as we note from **Fig. 4.3**, the radial composite and propagating permeability solutions converge at "late times," — *i.e.*, when the reservoir permeability dominates the pressure response. This is an important validation as the models do agree uniquely at late times. We conclude that this comparison suggests utility of our new model for the analysis of well test data in gas condensate reservoirs — with the caveat that we noted earlier regarding the fact that our proposed model uses a single value of diffusivity, and the 2-zone composite reservoir model uses 2 distinct diffusivities (*i.e.*, the "near well" and the "reservoir" diffusivi-ties).

The issue of the "sealing faults" model is somewhat more complex — we will simply suggest that a "flow barrier" (*i.e.*, a sealing fault) and a flow contrast (*i.e.*, the 2-zone radial composite reservoir model and the propagating permeability model) have similar (though not identical) behavior because the flow barrier/ contrast affects the pressure behavior in a similar fashion. This conclusion is somewhat inductive, but we believe it is both plausible and relevant.

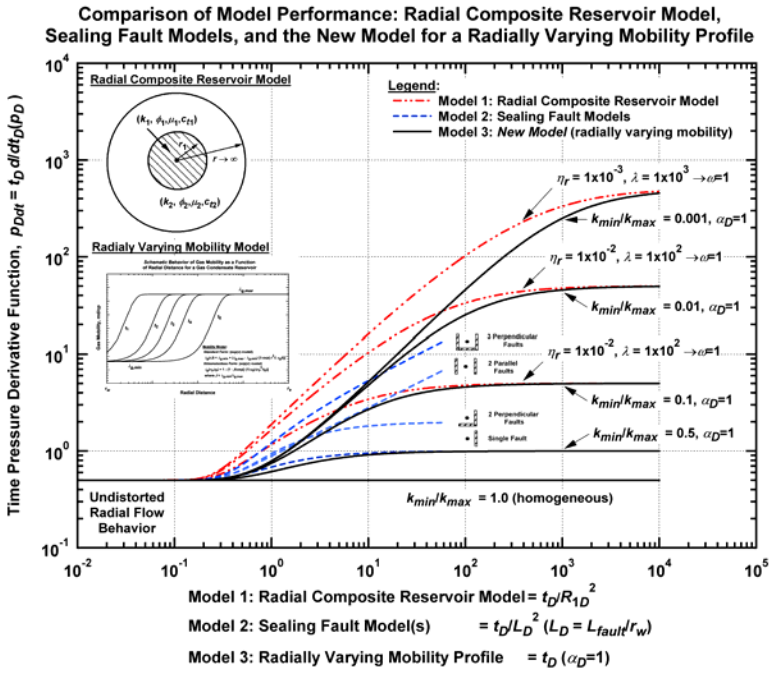

Figure 4.3 – Combined pressure derivative type curve for the following cases: sealing faults, a single radial composite region, and the proposed model for a radially-varying mobility profile.

4.2 Validation of the New Solution — Literature Data

Pressure Behavior in Radial Distance — Literature Data (Roussennac ref. 1)

Case 1: Roussennac Fig 2.7 — our starting point for comparisons of literature data is the case presented as Fig. 2.7 by Roussennac,[1] where this particular case was for a pressure drawdown sequence performed in an infinite-acting gas condensate reservoir. In order to make a proper comparison of our new model with the data presented by Roussennac, we must utilize the *pseudopressure* function to account for variations in fluid properties at a function of pressure. Specifically, we will only utilize the pseudopressure formulation for the case of a dry gas — this approach would be the typical one employed in practice (*i.e.*, for well test analysis) and our goal is to establish our new (equivalent liquid) solution as a practical mechanism for analysis.

The definition of pseudopressure that we employ for the case of a dry gas is given as:

$$p_p = \frac{\mu_{gi} z_i}{p_i} \int_{p_{base}}^{p} \frac{p}{\mu_g z} dp \quad \text{.....(4.1)}$$

In evaluating Eq. 4.01 we require the z-factor and the gas viscosity as functions of pressure. We present the z-factor as a function of pressure in **Fig. 4.4a** and the gas viscosity as a function of pressure in **Fig. 4.4b.** In Figs. 4.4a and 4.4b we have provided both the original fluid property data provided by Roussennac (generated using an equation of state (EOS)) for this fluid mixture ("Mix 2"), as well as "dry gas" properties generated using simplified correlations. We note a reasonably good correlation of these functions and we comment that our purpose in generating the "dry gas" trends was to provide sufficient data for the calculation of the pseudopressure function (Roussennac only gave 5 data points for the gas density and gas viscosity functions for this case).

In **Fig. 4.4c** we provide the pseudopressure function computed using Eq. 4.01 and the z-factor and gas viscosity data obtained from the dry gas correlations. We note a very consistent trend for the pseudo-pressure function and we also observe that for the pressures greater than 3000 psia that $\Delta p_p \approx 1.002\ \Delta p$ — which clearly is a coincidence, one would not expect a near 1:1 ratio for these functions. This observation potentially simplifies our analysis/comparison of the data for this case (*i.e.*, we could simply use Δp data instead of Δp_p data) — however, we would like to provide as rigorous an analysis as possible, so we will use the Δp_p data functions. We again note that this situation (*i.e.*, $\Delta p_p \approx 1.002\ \Delta p$) is a coincidence, and we should not generalize any such observations. We will utilize the Δp_p data functions for all cases in this work (with the possible exception of cases where fluid property data are simply unavailable).

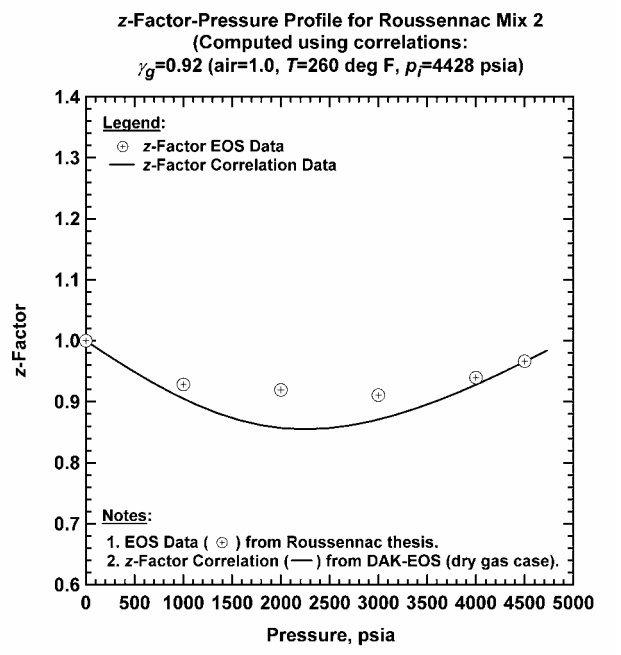

Figure 4.4a – z-factor profiles for the Roussennac[1] data case (Mix 2) — includes Roussennac EOS (simulation) data and data from dry gas correlation.

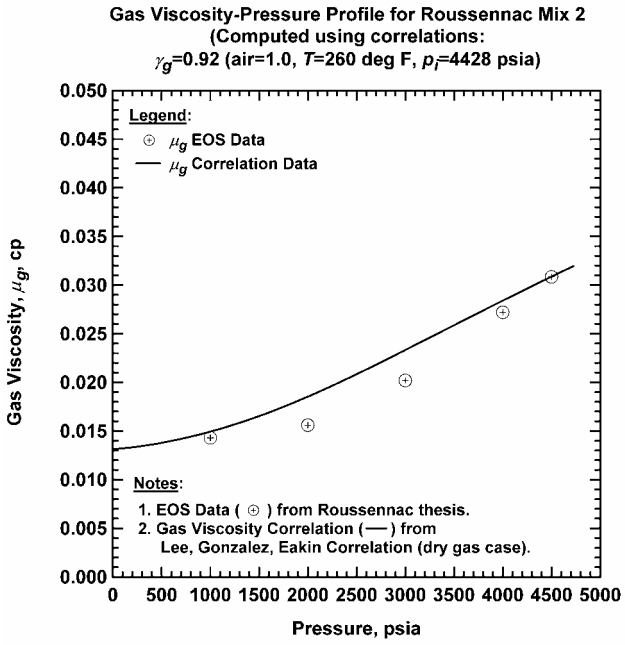

Figure 4.4b – Gas viscosity profiles for the Roussennac[1] data case (Mix 2) — includes Roussennac EOS (simulation) data and data from dry gas correlation.

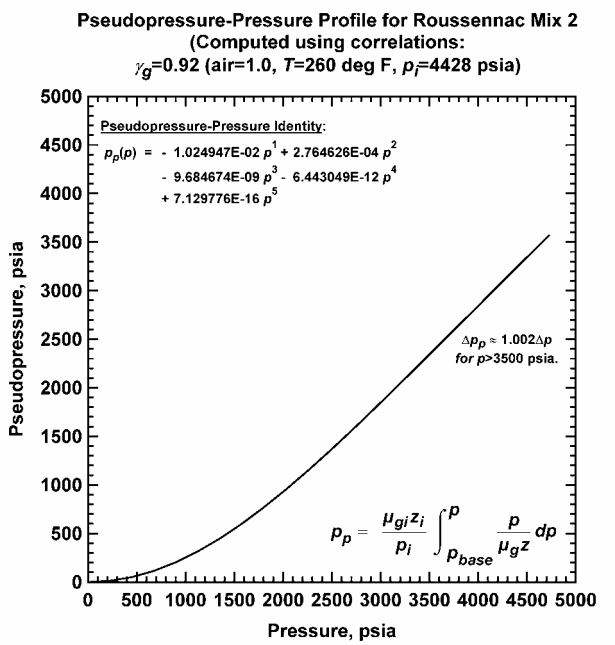

Figure 4.4c – Pseudopressure trend for the Roussennac[1] data case (Mix 2) — generated using the z-factor and gas viscosity data obtained from the dry gas correlations, and the pseudopressure definition given by Eq. 4.01.

To initiate the comparison of data cases, we first present a plot of p_p versus r in **Fig. 4.5**, where the pressure data were acquired using electronic digitization of Roussennac Fig. 2.7. We note that 5 separate cases are provided by Roussennac (*i.e.*, data trends for t= 0.0667, 1.1667, 5, 24, and 456 hours). We observe an apparent "propagation" of the pressure distribution into the reservoir — at this scale it is clear that the near-well pressure behavior is *not* linear with respect to the logarithm of radius (as are the results for the liquid case (see **Fig. 4.6**)) — we presume that this is an effect of the propagating radial profile of k_g/μ_g as well as the "compressibility effects" of the dry gas and gas condensate fluids. Regardless, we recognize that this particular plot cannot be "reconciled" with the liquid case.

Our next comparison is that of the Δp_p and $|\eta\, d\Delta p_p/d\eta|$ functions versus η (η=r^2/t) (**Fig. 4.7)**, where we note that use of the η-variable makes this plot consistent with our "type curves" (*i.e.*, **Figs. 3.2 and 3.3**). As we noted earlier, it would not be typical for the η-variable (η=r^2/t) to be used in practice (we are generally only interested in "t" behavior) — however, for the purposes of comparison for pressure distributions taken in the reservoir, use of the η-variable is logical (and preferred). In **Fig. 4.7** we note that the $|\eta\, d\Delta p_p/d\eta|$ function suffers somewhat because we have used the entire data trend (*i.e.*, Δp_p as a function of η).

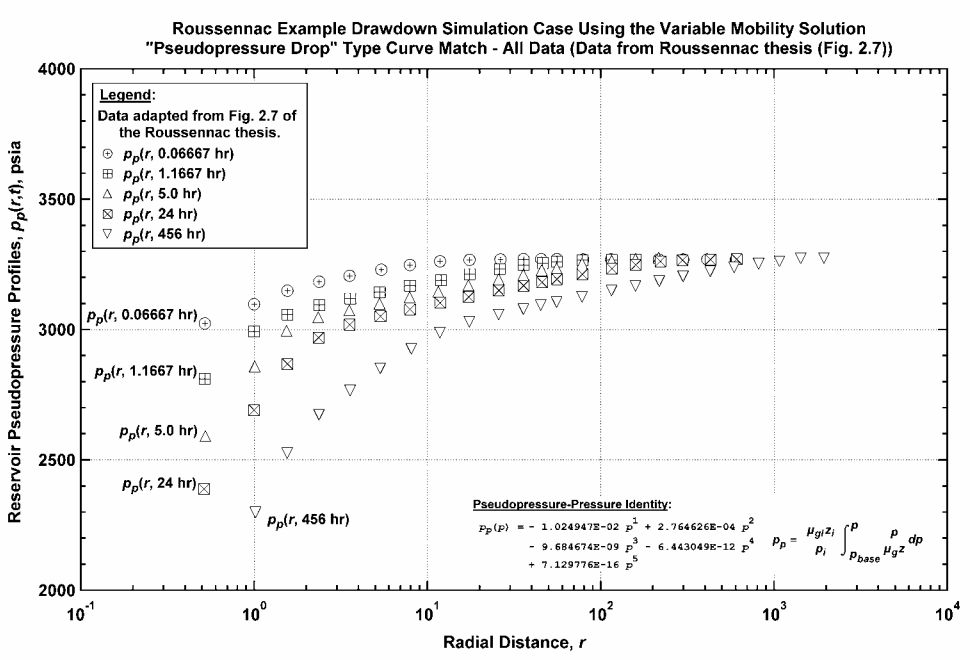

Figure 4.5 – p_p versus r for the Roussennac case of Fig. 2.7 — the pressure data were digitized and later converted to pseudopressure (p_p) using the transformation shown in **Fig. 4.4c**.

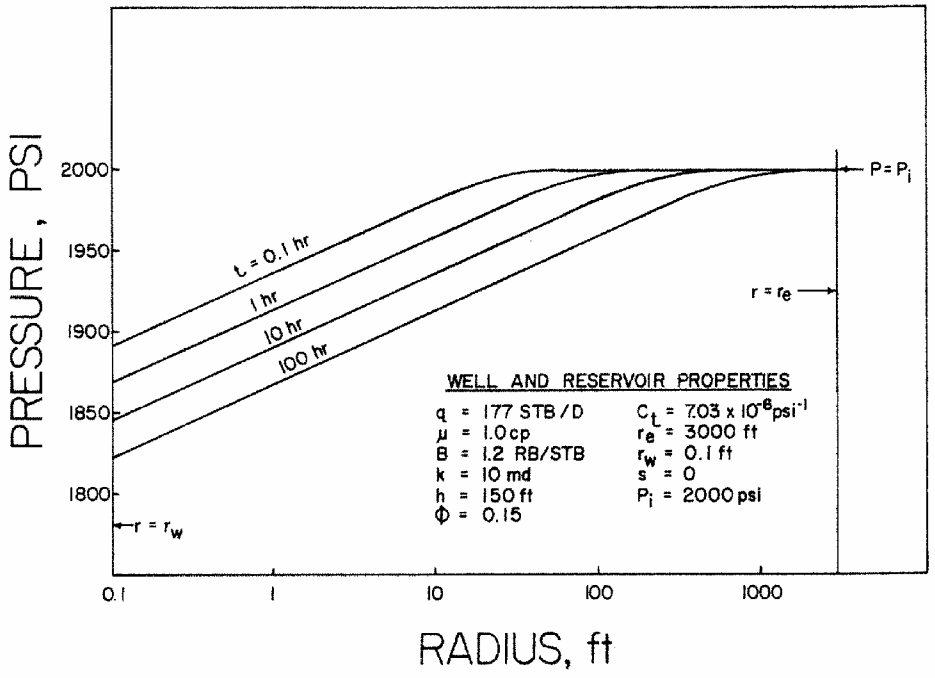

Figure 4.6 – Example case of p versus r for liquid flow — presented by Lee (ref. 18).

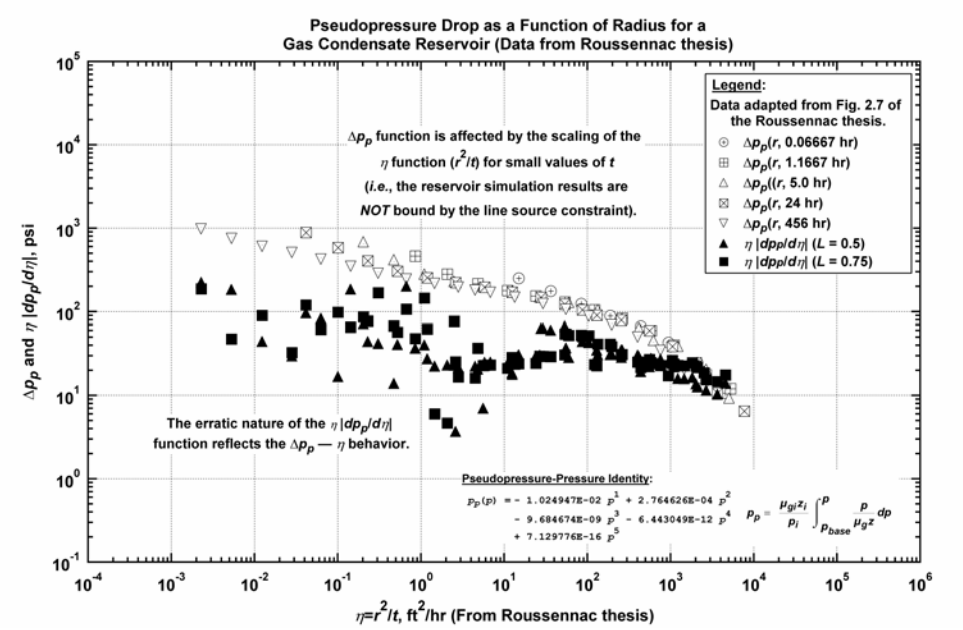

Figure 4.7 – Δp_p and $|\eta\, d\Delta p_p/d\eta|$ functions versus η for Roussennac Fig. 2.7 ($\eta=r^2/t$). The scatter in the $|\eta\, d\Delta p_p/d\eta|$ function is due to the Δp_p data not being uniquely "line source" in character (*i.e.*, these are numerical simulation results, and are not bound to the "line source" criterion).

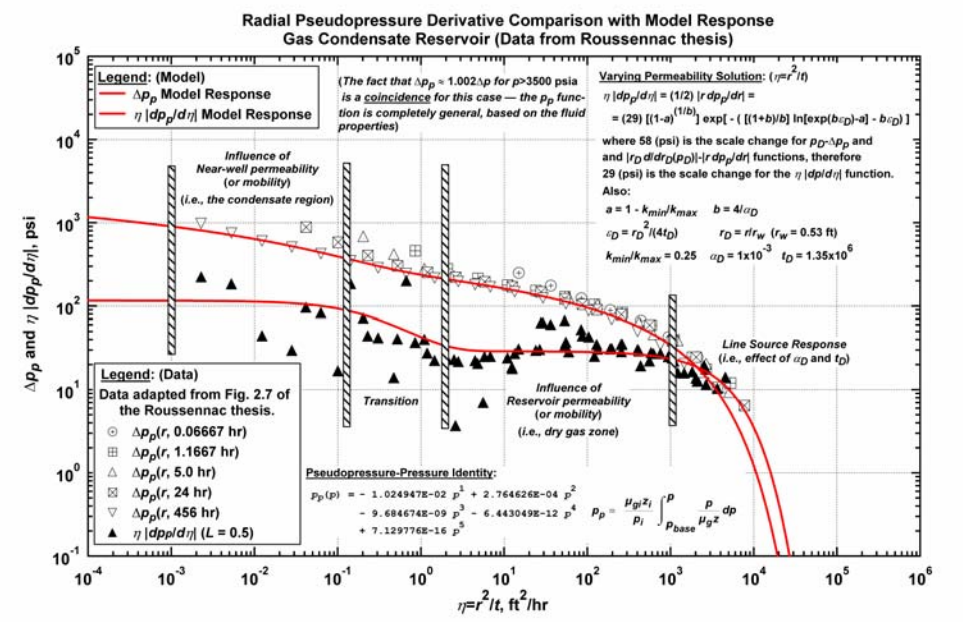

Figure 4.8 – Δp_p and $|\eta\, d\Delta p_p/d\eta|$ functions versus η ($\eta=r^2/t$) (data from Roussennac Fig. 2.7, model trends are derived from the new model for a varying mobility profile).

The "noise" in the $|\eta\, d\Delta p_p/d\eta|$ function is due to "incomplete" conversion of the numerical results to the "line source" case (*i.e.*, using the η-variable should convert "line source" data to a single trend — however, if the data are not perfectly line source data (as these simulated results are not), then the Δp_p - η trend will not be a perfect correlation (nor will the $|\eta\, d\Delta p_p/d\eta|$ - η trend)). This is not a major issue, simply a matter that requires explanation/orientation.

In **Fig. 4.8** we present the Δp_p and $|\eta\, d\Delta p_p/d\eta|$ data functions versus η ($\eta=r^2/t$), and then superimpose the "match" solution for Δp_p and $|\eta\, d\Delta p_p/d\eta|$ generated using our new variable-mobility model. We note very good agreement in the Δp_p functions (with the noted exception of the off-trend (*i.e.*, non-line source) data. Further, we also note reasonable agreement in the $|\eta\, d\Delta p_p/d\eta|$ model and data functions — where we again remark that the "scatter" in the $|\eta\, d\Delta p_p/d\eta|$ data function is due to our use of all of the Δp_p data in the derivative calculation (we did not edit out the off-trend data). Regardless of the data issues, we find a very reasonable overall match of the Δp_p and $|\eta\, d\Delta p_p/d\eta|$ functions — and we conclude that our model does appropriately represent the data for this particular case.

Case 2: Roussennac Fig 2.9 — We provide another validation of the new solution by comparison another data case presented by Roussennac (ref. 1). In this particular, this case includes a "skin zone" developed using a zone of altered permeability near the well. We note immediately that our solution does not include such a feature, and is not likely to reproduce such a feature (if even by coincidence, such an interpretation would be incorrect). Our goal is to demonstrate the utility of our new solution against another data case — in this particular case (as opposed to the previous data case) the only major change is the addition of the near-well skin zone. For reference, this case uses exactly the same fluid properties as the previous case (*i.e.*, Roussennac "Mix 2"), as such, the pseudopressure transformation for this case is identical to that of the previous case.

In **Fig. 4.9a** we present the p_D—Δp_p match for this case and the p_{Ddr}—$|r(d\Delta p_p/dr)|$ match is shown in **Fig. 4.9b**. With the exception of the behavior near the well, we note an excellent match of the data with the proposed solution. The behavior at small values of r is dominated by the "skin zone" — where the "skin zone" is actually a region of specified permeability used to provide the effect of near-well damage. As noted, we do not consider the existence of a "near-well damage" zone, we simply model a propagating permeability profile as shown in **Fig. 1.2**.

In **Fig. 4.10** we present the Δp_p and $|r(d\Delta p_p/dr)|$ data along with the Δp_p and $|r(d\Delta p_p/dr)|$ functions computed using our new reservoir model. Using **Fig. 4.10** we have attempted to identify/classify the flow regimes which were observed during this simulation. We note that this comparison provides a strong validation of our proposed solution for the case of a variable mobility profile.

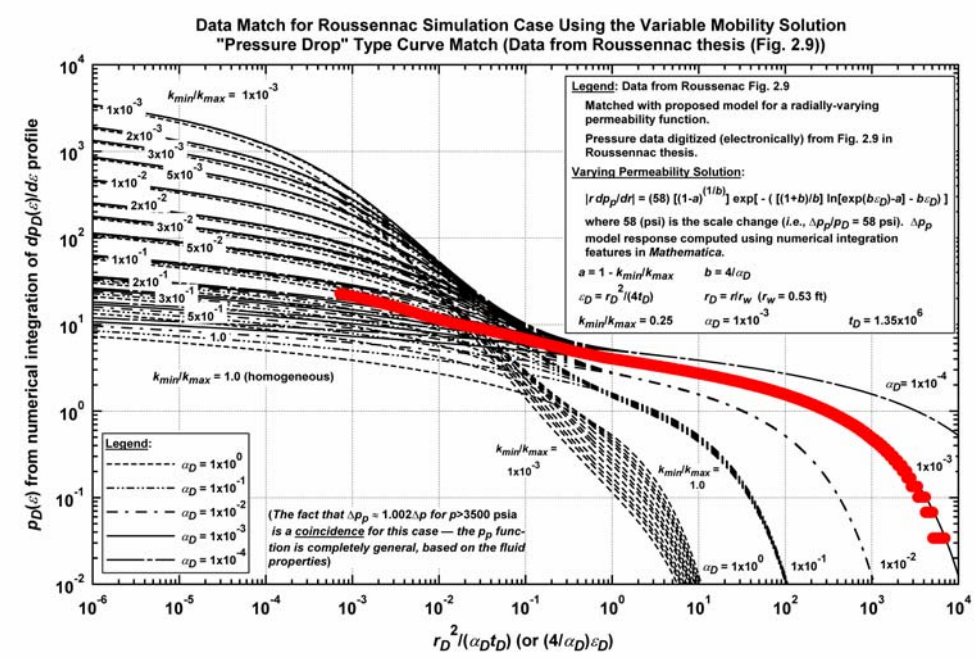

Figure 4.9a – Match of Roussenac[1] data (digitized) and the new variable mobility model (type curve match) — $p_D(\varepsilon_D)$ versus $(\alpha_D t_D)/r_D^2$ format.

Pressure Behavior in Radial Distance — Literature Data (Vo ref. 19)

Case 3: Vo[19] Fig 3.1 — As with the cases presented by Roussennac, we use the literature case presented by Vo to validate our proposed solution for the case of a radially varying mobility profile. This case presented by Vo does not include skin effects and should be modeled well by our proposed solution. As with the cases presented by Roussennac, we use the *pseudopressure* function to account for variations in fluid properties at a function of pressure. We again use the pseudopressure formulation for the case of a dry gas (see **Figs. 4.11a-4.11c**) — where the pseudopressure function (**Fig. 4.11.c**) is computed using *z*-factor data (**Fig. 4.11.a**) and gas viscosity data (**Fig. 4.11.b**) obtained from the equation-of-state (EOS) that Vo used to model this fluid mixture (*i.e.*, Vo "Fluid 2" (ref. 19)).

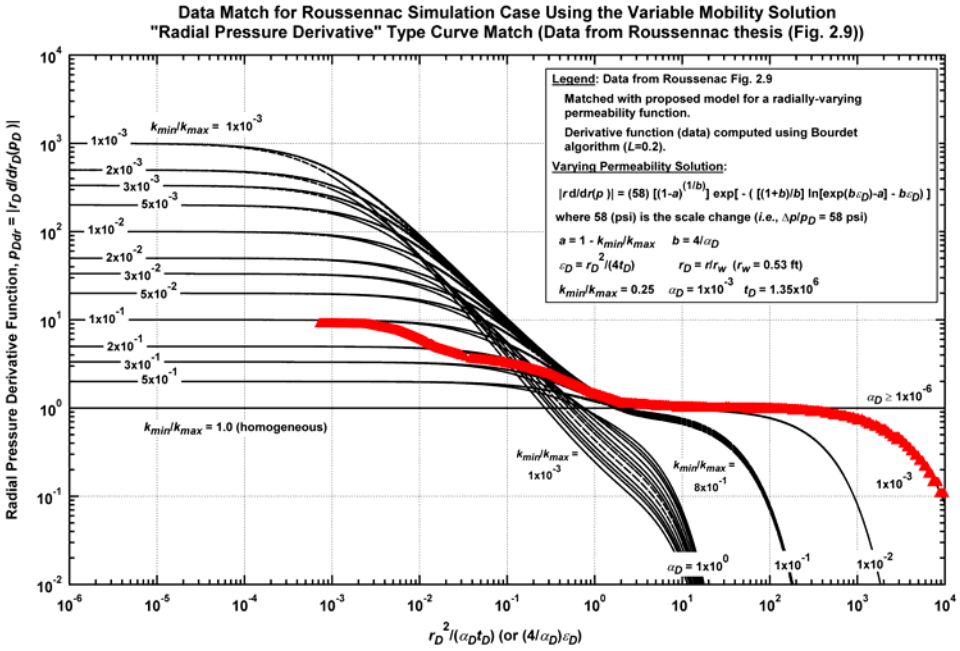

Figure 4.9b – Match of Roussenac[1] data (digitized) and the new variable mobility model (type curve) — $|r_D(\partial p_D/\partial t_D)|$ versus $(\alpha_D t_D)/r_D^2$ format.

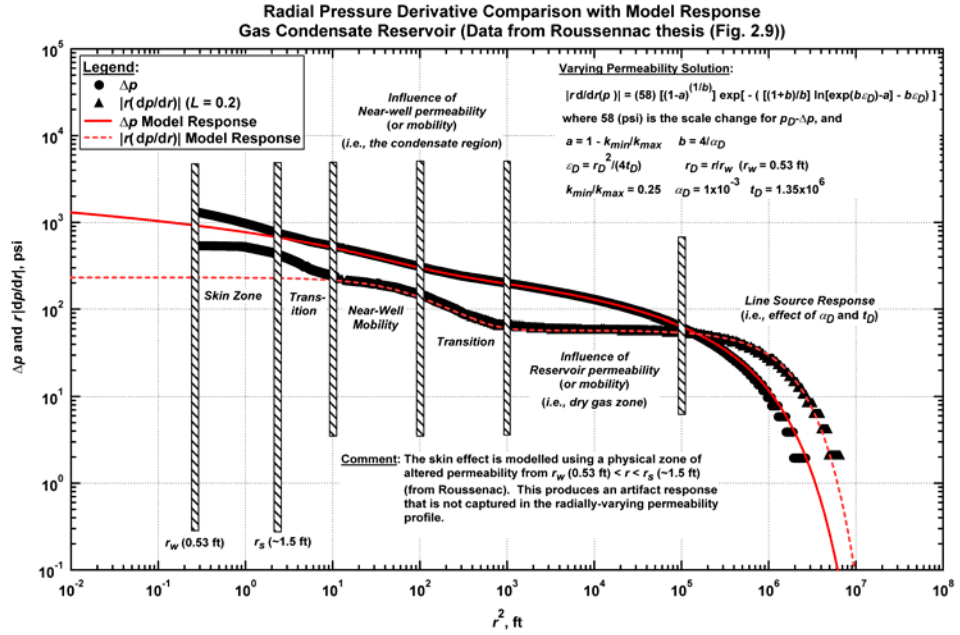

Figure 4.10 – Match of Roussenac[1] data (digitized) and the new variable mobility model (data/model match) — Δp and $r|dp/dr|$ versus r^2 format.

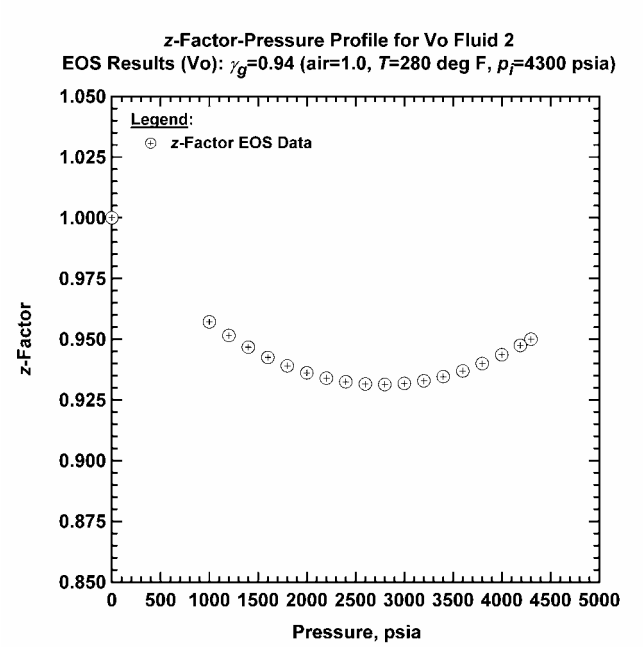

Figure 4.11a– z-factor profiles for the Vo[19] data case (Fluid 2) — Vo EOS (simulation) data.

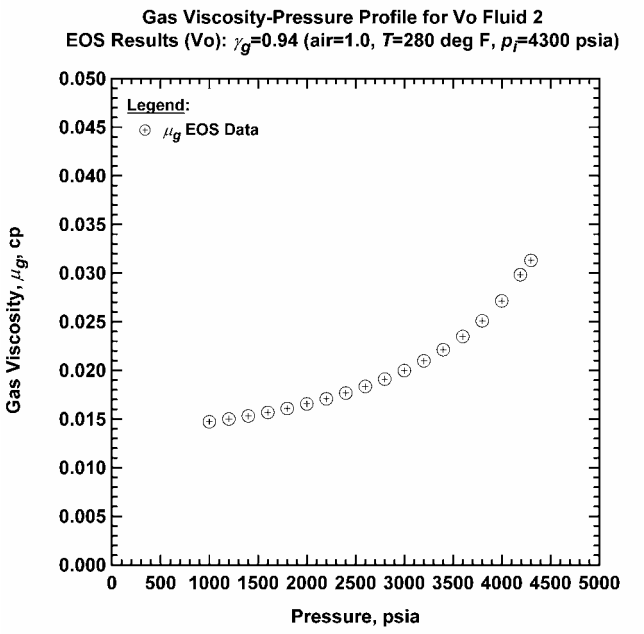

Figure 4.11b– Gas viscosity profiles for the Vo[19] data case (Fluid 2) — Vo EOS (simulation) data.

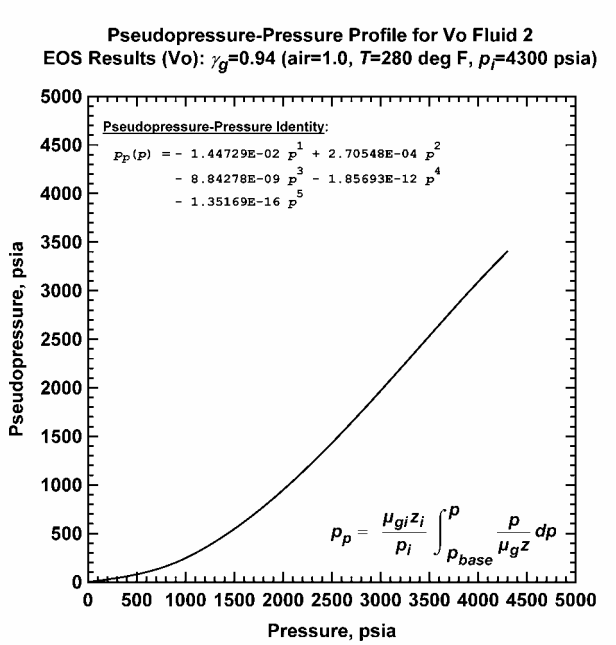

Figure 4.11c– Pseudopressure trend for the Vo[19] data case (Fluid 2) — generated using the z-factor and gas viscosity data obtained from Vo EOS calculations, and the pseudopressure definition given by Eq. 4.01.

In **Fig. 4.12** we present the Δp_p and $|r(d\Delta p_p/dr)|$ data for the Vo case along with the Δp_p and $|r(d\Delta p_p/dr)|$ model functions computed using our new reservoir model (this plot illustrates the "best match" of the Vo data with our new model). As for the Roussennac cases, we again identify/classify the flow regimes which were observed during this simulation for the Vo case. We note an exceptional match of all data and model functions for the Vo case, providing further validation of our new model for the case of a radially varying mobility model.

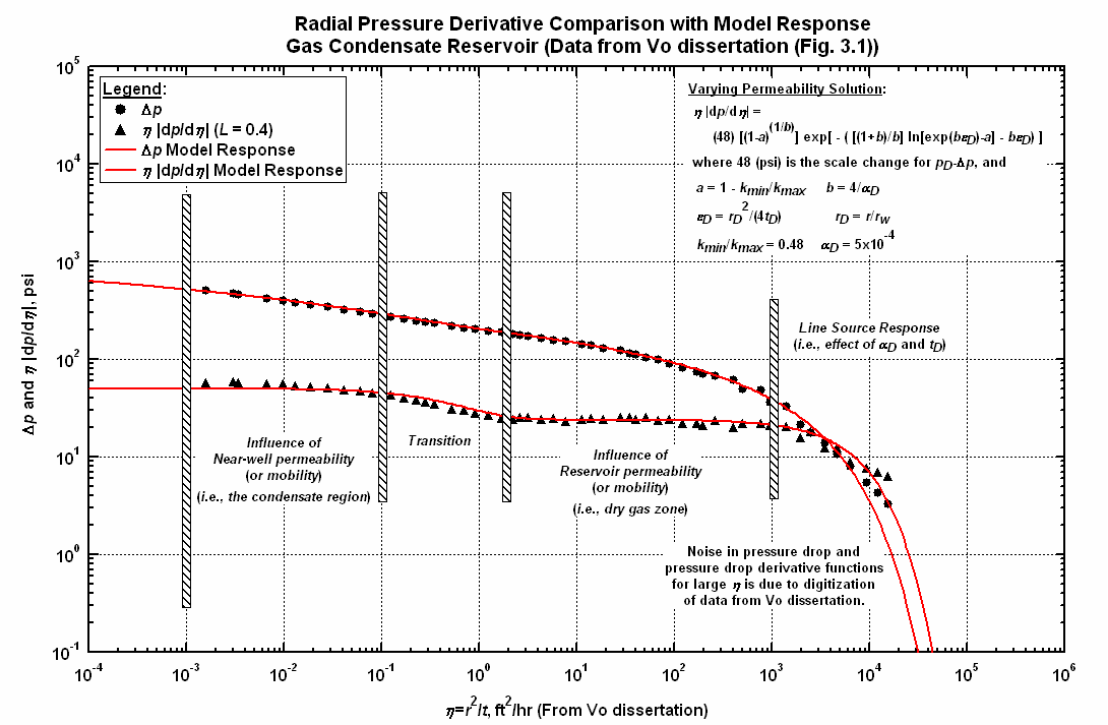

Figure 4.12– Match of Vo[19] data (digitized) and the new variable mobility model (data/model match) — Δp_p and $\varepsilon|d\Delta p_p/d\varepsilon|$ versus η ($\eta = r^2/t$) format. (s=0).

CHAPTER V
SUMMARY, CONCLUSIONS, AND RECOMMENDATIONS FOR FUTURE WORK

5.1 Summary

We have developed and validated a new solution for the case of a radially varying permeability profile in an infinite-acting reservoir. We believe that this result can be applied towards the analysis and interpretation of reservoir performance data obtained from wells in gas condensate reservoirs.

Our validation of this new solution utilized comparisons with reference data (numerical simulation results) obtained from the petroleum literature. We used pressure-radius data which illustrate the development of the condensate bank and we also computed auxiliary functions such as pseudopressure and the pressure derivative functions in order to enhance/illustrate certain characteristic features.

We also compared our new model to pressure derivative—time profiles for wells in radial composite reservoir systems and for wells in systems with one or more sealing faults. These comparisons were used to establish the similarity of the pressure derivative functions for certain cases with the pressure derivative functions given by our new solution. For orientation with field data, we also generated a variety of cases which include wellbore storage effects. These cases are designed to illustrate the relative impact of wellbore storage effects on the solution for a radially varying mobility profile — our primary conclusion is that wellbore storage and varying mobility influences generate responses which could be confused with other reservoir features (*e.g.*, dual porosity reservoir effects).

5.2 Conclusions

The following conclusions are made based on the results obtained from this work

1. New Solution: We have proposed, developed, and verified new solutions (for pressure and the pressure derivative functions in terms of radial distance and time) for the case of a well producing at a constant flowrate from an infinite-acting radial flow system where the permeability varies in radial distance and time (see Eq. 1.1).

$$k = k_{min} + (k_{max} - k_{min}) \left[1 - \exp\left[\frac{-1}{\alpha} \frac{r^2}{t} \right] \right] \quad \text{.....(1.1)}$$

Eq. 1.1 is proposed based on observations of well performance behavior derived from numerical simulation of the gas phase for a radial gas condensate reservoir system.

The relevant results developed in this work are given by Eqs. 3.14 and 3.15:

$$\varepsilon_D \frac{dp_D}{d\varepsilon_D} = -\frac{1}{2}(k_{min}/k_{max})^{\frac{\alpha_D}{4}} \exp\left[-\frac{(1+\frac{4}{\alpha_D})}{\frac{4}{\alpha_D}} \ln\left[e^{-\frac{4}{\alpha_D}\varepsilon_D} - (1-k_{min}/k_{max}) \right] + \frac{4}{\alpha_D}\varepsilon_D \right]$$

("derivative" form) ..... (3.14)

$$p_D(\varepsilon_D) = \frac{1}{2}(k_{min}/k_{max})^{\frac{\alpha_D}{4}} \int_{\varepsilon_D}^{\infty} \left[\frac{1}{\varepsilon_D} \exp\left[-\frac{(1+\frac{4}{\alpha_D})}{\frac{4}{\alpha_D}} \ln\left[e^{-\frac{4}{\alpha_D}\varepsilon_D} - (1-k_{min}/k_{max}) \right] + \frac{4}{\alpha_D}\varepsilon_D \right] \right] d\varepsilon_D$$

("pressure" form) ..... (3.15)

We note that Eq. 3.15 cannot be resolved beyond the integral formulation as presented. As such, all results for Eq. 3.15 are generated using numerical integration of Eq. 3.14 performed in *Mathematica*. The derivative formulation given by Eq. 3.14 is a closed form result — and is computationally efficient.

Alternate forms of Eq. 3.14, written in terms of r_D and t_D are given as:.

$$-r_D \frac{\partial p_D}{\partial r_D} = (k_{min}/k_{max})^{\frac{\alpha_D}{4}} \exp\left[-\frac{(1+\frac{4}{\alpha_D})}{\frac{4}{\alpha_D}} \ln\left[e^{-\frac{4}{\alpha_D}\varepsilon_D} - (1-k_{min}/k_{max}) \right] + \frac{4}{\alpha_D}\frac{r_D^2}{4t_D} \right]$$

("r_D derivative" form) ..... (3.16)

$$t_D \frac{\partial p_D}{\partial t_D} = \frac{1}{2}(k_{min}/k_{max})^{\frac{\alpha_D}{4}} \exp\left[-\frac{(1+\frac{4}{\alpha_D})}{\frac{4}{\alpha_D}} \ln\left[e^{-\frac{4}{\alpha_D}\varepsilon_D} - (1-k_{min}/k_{max}) \right] + \frac{4}{\alpha_D}\frac{r_D^2}{4t_D} \right]$$

("t_D derivative" form) ..... (3.17)

2. Comparison/Validation: The proposed solution is presented in comparison to numerical simulation results (for the $\partial p_D/\partial r_D$ formulation). The $\partial p_D/\partial t_D$ formulation is compared to the 2-zone radial composite model as well as simplified cases of "sealing faults" — the comparisons indicate that the proposed solution does produce similar features and suggests the model would be an effective interpretation tool for well test analysis.

   Our presentation of the $p_{wD}(t_D)$ and $p_{wDd}(t_D)$ functions (which include wellbore storage and skin effects) indicate that the influence of the α (or α_D) parameter and the k_{min}/k_{max} ratio is substantive and unique for certain cases (*e.g.*, low values of C_D), while for higher values of C_D wellbore storage effects dominate the response. This is analogous to say, the case of well performance in a dual porosity/naturally fractured reservoir.

3. Pressure Buildup Case: This is a case for future investigation, our efforts to resolve the pressure buildup case using conventional methods yielded inconclusive results. This situation may be a product of using (or misusing) the superposition theorem, and/or some other mitigating factor(s). Regardless, this topic (*i.e.*, the pressure buildup case) warrants further investigation.

5.3 Limitations and Recommendations

Limitations:

1. The major limitation of our new solution is that the pressure buildup case must be addressed. Our attempts to date (using superposition) are not sufficient — we must incorporate the change in rate (and the change in the $k_g(r,t)$ profile) directly in the solution formulation.
2. While we do address the $k_g(r,t)$ profile directly in this work, we also need to address the changes in diffusivity ($k_g/(\phi\mu_g c_g)$) which occur in terms of both radius and time.

Recommendations:

1. Future work should address the pressure buildup case and the variation in diffusivity.
2. Well testing practices should be implemented with an emphasis on acquiring the most representative pressure data possible. Diagnosis of the condensate bank using near-well saturations (from well logs) remains elusive, so we must continue to rely (primarily) on pressure information.

NOMENCLATURE

Field Variables (*Pressure, Formation, and Fluid Properties*)

B = Formation volume factor, RB/STB

c_g = Gas compressibility, psi^{-1}

c = Isothermal compressibility, psi^{-1}

c_f = Pore compressibility, psi^{-1}

c_t = Total compressibility, psi^{-1}

h = Net pay thickness, ft

k or k_g = Effective permeability for gas, md

k_{max} = Maximum effective permeability to gas, md

k_{min} = Minimum effective permeability to gas, md

p_i = Initial reservoir pressure, psia

p_{res} = Reservoir pressure, psia

p_{dew} = Dewpoint pressure, psia

p_{wf} = Flowing pressure, psia

p_{ws} = Shut-in pressure, psia

p_p = Pseudopressure, psia

q = Flowrate, STB/D

q_{sf} = "Sandface" flowrate, STB/D

q_{sur} = "Surface" flowrate, STB/D

r_w = Wellbore radius, ft

r = Radial distance, ft

t = Time, hr

t_p = Production time, hr

Δt = Shut-in Time, hr

α = Scaling term for pressure behavior, $(cp\text{-}psi^{-1})/md$

ε = Boltzmann transform variable ($r^2/(4t)$)

μ = Viscosity, cp

ϕ = Porosity

λ = Mobility (mD/cp)

R_p = Cumulative Gas Oil Ratio, (scf(gas)/stb(oil))

R_s = Solution (Dissolved) Gas Oil Ratio, (scf(gas)/stb(oil))

DimensionlessVariables

C_D = Dimensionless wellbore storage coefficient

k_D = Dimensionless permeability function

p_D = Dimensionless pressure (generic)

p_{Ddr} = Dimensionless pressure derivative function in radial distance (Eq. 8)

p_{Ddt} = Dimensionless pressure derivative function in time (Eq. 7)

p_{sD} = p_D+s, Dimensionless pressure with skin effects

p_{wD} = Dimensionless pressure with wellbore storage and skin effects

p_{wDdt} = Dimensionless pressure derivative function in time including wellbore storage and skin effects

q_{Dwbs} = Dimensionless flowrate for wellbore storage

r_D = Dimensionless radius

t_D = Dimensionless time

t_{pD} = Dimensionless production time

Δt_D = Dimensionless shut-in time

ε_D = Dimensionless Boltzmann transform variable

a_D = Dimensionless empirical scaling term for pressure behavior

s = Skin factor, dimensionless

REFERENCES

1. Roussennac, B.: "Gas Condensate Well Analysis," M.S. thesis, Stanford University, Stanford, California (2001).
2. *Mathematica* (software) Version 4.1, Wolfram Research, Champaign-Urbana, IL (2001).
3. Carslaw, H.S.; Jaeger, J.C.: *Conduction of Heats in Solids* (second edition), Oxford University Press, New York (1959).
4. Ramey, H.J.; "Approximate Solutions for Unsteady Liquid Flow in Composite Reservoirs", *Journal of Canadian Petroleum Technology*, (January-March 1970), Montreal , 32-37.
5. Jones, J.R.: "Computation and Analysis of Single Well Responses for Gas Condensate Systems," Ph.D. dissertation, The University of Tulsa, Tulsa, Oklahoma (1985).
6. Bóe, A., Skjaoveland, S.M., Whitson, C.H: "Two Phase Two Phase Pressure Test Analysis," *SPE Formation Evaluation* (December 1989), 601-610.
7. Al-Hussainy, R., Ramey, H.J., Jr., and Crawford, P.B.: "The Flow of Real Gases Through Porous Media," *JPT* (May 1966) 624-36, *Trans*., AIME, **237**.
8. Agarwal, R.G.: "Real Gas Pseudo-Time — A New Function for Pressure Buildup Analysis of MHF Gas Wells," paper SPE 8729 presented at the 1979 SPE Annual Technical Conference and Exhibition, Las Vegas, 23-26 September.
9. Xu, S.; Lee, W.J.: "Two Phase Well Test Analysis of Gas Condensate Reservoirs," paper SPE Paper 56483 presented at the 1999 SPE Annual Technical Conference and Exhibition; Houston, Texas, 3-6 October.
10. Raghavan, R., Chu, W., and Jones, J.R.: "Practical Considerations in the Analysis of Gas Condensate Well Tests," paper SPE 30576 presented at the 1995 SPE Annual Fall Technical Conference and Exhibition, Dallas, Texas, 22-25 October.
11. Fevang, O. and Whitson, C.H.: "Modeling Gas Condensate Well Deliverability," *SPE Reservoir Engineering* (November 1996), 221.
12. Jones, J.R. and Raghavan, R.: "Interpretation of Flowing Well Responses in Gas-Condensate Wells," *SPE Formation Evaluation* (September 1988) 578-594.
13. Jones, J. R. and Vo, D.T., and Raghavan, R: "Interpretation of Pressure Build Up Responses in Gas-Condensate Wells," *SPE Formation Evaluation* (March 1989) 93-104.

14. Stewart, G., Gupta, A., and Westaway, P.: "The Interpretation of Interference Tests in a Reservoir with Sealing and Partially Communicating Faults," paper SPE 12967 presented at the 1984 European Petroleum Conference, London, 25-28 October.

15. Raghavan, R.: *Well Test Analysis*, Prentice-Hall, Upper Saddle River, NJ (1993) 154-158.

16. Blasingame, T.A., Johnston, J.L., and Lee, W.J.: "Advances in the Use of Convolution Methods in Well Test Analysis," paper SPE 21826 presented at the 1991 Joint Rocky Mountain Regional/Low Permeability Reservoirs Symposium, Denver, Colorado, 15-17 April.

17. Tang, R.W. and Brigham, W.E.: *Transient Pressure Analysis in Composite Reservoirs*, Topical Report SUPRI TR-31 (1982).

18. Lee, W.J.: *Well Testing*, Society of Petroleum Engineers, Richardson, TX (1982).

19. Vo, D.T.: "Well Test Analysis for Gas Condensate Reservoirs," Ph.D. dissertation, The University of Tulsa, Tulsa, Oklahoma (1989).

APPENDIX A

DERIVATION OF THE PRESSURE DERIVATIVE FUNCTIONS WITH RESPECT TO TIME AND RADIUS FOR THE CASE OF A RADIALLY VARYING PERMEABILITY PROFILE (EQUIVALENT LIQUID CASE)

In this Appendix, we derive two expressions for the pressure derivative (time and radial distance formulations) that consider the changing effective (or relative) permeability of the retrograde gas as condensate evolves with decreasing pressure.

This derivation begins with the base diffusivity equation — *i.e.*, the partial differential equation which describes the flow of a single phase fluid in a porous medium with respect to time and distance. The effective permeability to gas in such cases will not be constant, but is dependent on the PVT and rock-fluid properties. The primary contribution of this work is the development of a closed form analytical solution for the case of a radially varying mobility (or effective permeability) function in a reservoir system. The subordinate contribution (which is, in some ways, more important than the solution) is our proposal of a simple functional relationship to represent the time and space-dependency of the gas mobility (or permeability) function.

The base form of the diffusivity equation that considers a varying permeability with respect to radius is given as:

$$\frac{1}{r}\frac{\partial}{\partial r}\left[kr\frac{\partial p}{\partial r}\right]=\frac{1}{0.0002637}\phi\mu c_t\frac{\partial p}{\partial t}\ \text{(Field units)} \quad \text{(A.1)}$$

As mentioned above, we have proposed a general model for the behavior of the permeability to gas as a function of time and radius. Our proposed model is given in its 2 most basic forms as:

$$k=k_{min}+(k_{max}-k_{min})\left[1-\exp\left[\frac{-1}{\alpha}\frac{r^2}{t}\right]\right] \quad \text{(A.2a)}$$

$$k=k_{max}-(k_{max}-k_{min})\exp\left[\frac{-1}{\alpha}\frac{r^2}{t}\right] \quad \text{(A.2b)}$$

We note that the α-parameter in Eqs. A.2a and A.2b is an empirical constant, most likely related to the PVT characteristics of the reservoir fluid, as well as the rock-fluid proper-ties. Our goal is not to assess the nature of the α-parameter, but rather, to use this as a mechanism to represent a complex process with a simple model. Eq. A.2b is the primary form used in this Appendix, and we will note that Eqs. A.2a and

A.2b have been validated conceptually via comparison with simulated performance for a gas condensate reservoir system.

We consider the Boltzmann transform, which allows us to relate dimensionless time and distance:

$$\varepsilon_D = \frac{r_D^2}{4t_D} \quad \text{(A.3)}$$

$$\frac{r^2}{\alpha t} = \frac{r_D^2}{\alpha_D t_D} \quad \text{(A.4)}$$

Substituting Eq. A.3 and Eq. A.4 into Eq. A.2b yields:

$$k = k_{max} - (k_{max} - k_{min}) \exp\left[\frac{-4}{\alpha_D}\varepsilon_D\right] \quad \text{(A.5)}$$

Defining a "dimensionless" permeability, k_D, we have:

$$k_D = k/k_{max} \quad \text{(A.6)}$$

or, in terms of the permeability, we obtain:

$$k = k_{max} k_D$$

We note that we will use the terms "permeability" and "effective permeability" interchangeably in this derivation — however, the variable in question is always *effective* permeability.

Substituting the definition of "dimensionless" permeability (*i.e.*, Eq. A.6) into Eq. A.5 gives us:

$$k_D = 1 - \left[1 - \frac{k_{\min}}{k_{\max}}\right] \exp\left[\frac{-4}{\alpha_D}\varepsilon_D\right] \quad \text{(A.7)}$$

We need to transform Eq. A.1 into dimensionless form — hence; we state the dimensionless variables used in this work are as follows: (Field units formulation)

Dimensionless Pressure:

$$p_D = \frac{1}{141.2}\frac{k_{max} h}{qB\mu}(p_i - p) \quad \text{(A.8)}$$

Dimensionless Time:

$$t_D = 0.0002637\frac{k_{max}}{\phi\mu c_t r_w^2} t \quad \text{(A.9)}$$

Dimensionless Radius:

$$r_D = \frac{r}{r_w} \quad \text{(A.10)}$$

Substituting Eqs A.9 and A.10 into Eq. A.4 and solving for the α_D parameter, we have:

$$\alpha_D = \frac{r_D^2}{r^2}\frac{t}{t_D}\alpha = \frac{1}{0.0002637}\frac{1}{r_w^2}\frac{\phi\mu c_t r_w^2}{k_{max}}\alpha$$

Or,

$$\alpha_D = \frac{1}{0.0002637}\frac{\phi\mu c_t}{k_{max}}\alpha \quad \text{..... (A.11)}$$

From Eq. A.11 we note that the α-parameter has the units of inverse diffusivity (*i.e.*, diffusivity ($k/(\phi\mu c_t)$) has the units of (md/(cp-psi^{-1}) — field units formulation) — therefore, α has the units of (cp-psi^{-1})/md. Physically, we assign the properties of the fluid and rock-fluid interaction to the α-parameter — however, we consider α to be an empirical parameter, and, as such, we should not attempt to quantify the components of α, but rather, we should simply use α to qualify the influence of the fluid on the permeability profile.

Substituting Eqs A.6, A.8-.10 into Eq. A.1 and rearranging yields the diffusivity equation in dimensionless form:

$$\frac{1}{r_D}\frac{\partial}{\partial r_D}\left[k_D r_D \frac{\partial p_D}{\partial r_D}\right] = \frac{\partial p_D}{\partial t_D} \quad \text{..... (A.12)}$$

We note that for the case where $k = k_{max}$, Eq. A.12 reverts to the conventional diffusivity equation for a constant permeability. We also note that we have assumed a slightly compressible fluid (*i.e.*, a liquid) in the derivation of the diffusivity equation for radial flow (*i.e.*, Eq. A.1). The assumption of a "liquid" may seem incompatible with the concept of a gas case — however, we are deriving a formulation for a "liquid" that will, in turn, be used for gases where the conventional gas pseudo-functions will be employed (*i.e.*, pseudopressure and pseudo-time). Simply put, this case represents an "equivalent" liquid, modifications will be addressed using pseudofunctions that "convert" the case in question to the "equivalent" liquid case.

Utilizing the Boltzmann transform we derive a relationship for pressure with respect to time and radius which includes the prescribed varying permeability model (*i.e.*, Eq. A.2 or A.7).

For convenience, we define the constants *a* and *b* as follows:

$$a = (1 - k_{min}/k_{max}) \quad \text{..... (A.13)}$$

$$b = \frac{4}{\alpha_D} \quad \text{..... (A.14)}$$

Substituting Eqs. A.13 and A.14 into Eq. A.7 yields:

$$k_D = 1 - a\,exp[-b\varepsilon_D] \quad \text{..... (A.15)}$$

Applying the product rule to the left-hand-side (LHS) of Eq. A.12 we have:

$$\frac{1}{r_D}\left[r_D \frac{\partial p_D}{\partial r_D}\frac{\partial k_D}{\partial r_D} + k_D \frac{\partial p_D}{\partial r_D}\frac{\partial r_D}{\partial r_D} + k_D r_D \frac{\partial}{\partial r_D}\left[\frac{\partial p_D}{\partial r_D}\right]\right] = \frac{\partial p_D}{\partial t_D}$$

Multiplying through the left-hand-side by $1/r_D$ gives:

$$\frac{\partial k_D}{\partial r_D}\frac{\partial p_D}{\partial r_D}+\frac{k_D}{r_D}\frac{\partial p_D}{\partial r_D}+k_D\frac{\partial}{\partial r_D}\left[\frac{\partial p_D}{\partial r_D}\right]=\frac{\partial p_D}{\partial t_D}$$

Collecting like terms and consolidating the k_D terms:

$$\frac{\partial k_D}{\partial r_D}\frac{\partial p_D}{\partial r_D}+k_D\left[\frac{\partial}{\partial r_D}\frac{\partial p_D}{\partial r_D}+\frac{1}{r_D}\frac{\partial p_D}{\partial r_D}\right]=\frac{\partial p_D}{\partial t_D}$$

..... (A.16)

Utilizing the chain rule to transform the r_D and t_D terms into the Boltzmann variable, ε_D, we have the following general formulation:

$$\frac{\partial y}{\partial x}=\frac{\partial \varepsilon_D}{\partial x}\frac{dy}{d\varepsilon_D}$$

Applying the chain rule on a term-by-term basis:

$$\frac{\partial k_D}{\partial r_D}=\frac{\partial \varepsilon_D}{\partial r_D}\frac{dk_D}{d\varepsilon_D}$$

$$\frac{\partial p_D}{\partial r_D}=\frac{\partial \varepsilon_D}{\partial r_D}\frac{dp_D}{d\varepsilon_D}$$

$$\frac{\partial p_D}{\partial t_D}=\frac{\partial \varepsilon_D}{\partial t_D}\frac{dp_D}{d\varepsilon_D}$$

Substituting these results into Eq. A.16 and rearranging, we have:

$$\left[\frac{\partial \varepsilon_D}{\partial r_D}\frac{dk_D}{d\varepsilon_D}\right]\left[\frac{\partial \varepsilon_D}{\partial r_D}\frac{dp_D}{d\varepsilon_D}\right]$$
$$+k_D\left[\frac{\partial \varepsilon_D}{\partial r_D}\frac{\partial}{\partial \varepsilon_D}\left[\frac{\partial \varepsilon_D}{\partial r_D}\frac{dp_D}{d\varepsilon_D}\right]+\frac{1}{r_D}\left[\frac{\partial \varepsilon_D}{\partial r_D}\frac{dp_D}{d\varepsilon_D}\right]\right]$$
$$-\left[\frac{\partial \varepsilon_D}{\partial t_D}\frac{dp_D}{d\varepsilon_D}\right]=0$$

Combining like terms,

$$\left[\frac{\partial \varepsilon_D}{\partial r_D}\right]^2\left[\frac{dk_D}{d\varepsilon_D}\frac{dp_D}{d\varepsilon_D}\right]+$$
$$k_D\left[\begin{array}{l}\dfrac{\partial \varepsilon_D}{\partial r_D}\dfrac{\partial}{\partial \varepsilon_D}\left[\dfrac{\partial \varepsilon_D}{\partial r_D}\dfrac{dp_D}{d\varepsilon_D}\right]\\ +\dfrac{1}{r_D}\left[\dfrac{\partial \varepsilon_D}{\partial r_D}\dfrac{dp_D}{d\varepsilon_D}\right]-\dfrac{1}{k_D}\left[\dfrac{\partial \varepsilon_D}{\partial t_D}\dfrac{dp_D}{d\varepsilon_D}\right]\end{array}\right]=0$$

Applying the product rule to the $\dfrac{\partial}{\partial \varepsilon_D}\left[\dfrac{\partial \varepsilon_D}{\partial r_D}\dfrac{dp_D}{d\varepsilon_D}\right]$ term,

$$\left[\frac{\partial \varepsilon_D}{\partial r_D}\right]^2\left[\frac{\partial k_D}{\partial \varepsilon_D}\frac{dp_D}{d\varepsilon_D}\right]+$$
$$k_D\left[\begin{array}{l}\dfrac{\partial \varepsilon_D}{\partial r_D}\dfrac{\partial \varepsilon_D}{\partial r_D}\dfrac{d^2 p_D}{d\varepsilon_D^2}+\dfrac{dp_D}{d\varepsilon_D}\dfrac{\partial \varepsilon_D}{\partial r_D}\dfrac{\partial}{\partial \varepsilon_D}\left[\dfrac{\partial \varepsilon_D}{\partial r_D}\right] \\ +\dfrac{1}{r_D}\left[\dfrac{\partial \varepsilon_D}{\partial r_D}\dfrac{dp_D}{d\varepsilon_D}\right]-\dfrac{1}{k_D}\left[\dfrac{\partial \varepsilon_D}{\partial t_D}\dfrac{dp_D}{d\varepsilon_D}\right]\end{array}\right]=0$$

Collecting like terms and isolating,

$$k_D\left[\begin{array}{l}\left[\dfrac{\partial \varepsilon_D}{\partial r_D}\right]^2\left[\dfrac{d^2 p_D}{d\varepsilon_D^2}\right]+ \\ \left[\dfrac{\partial}{\partial r_D}\left[\dfrac{\partial \varepsilon_D}{\partial r_D}\right]+\dfrac{1}{r_D}\dfrac{\partial \varepsilon_D}{\partial r_D}-\right. \\ \left.\dfrac{1}{k_D}\dfrac{\partial \varepsilon_D}{\partial t_D}+\left[\dfrac{\partial \varepsilon_D}{\partial r_D}\right]^2\dfrac{1}{k_D}\dfrac{dk_D}{d\varepsilon_D}\right]\dfrac{dp_D}{d\varepsilon_D}\end{array}\right]=0$$

Dividing through by $k_D\left[\dfrac{\partial \varepsilon_D}{\partial r_D}\right]^2$,

$$\frac{d^2 p_D}{d\varepsilon_D^2}+\left[\begin{array}{l}\dfrac{1}{\left[\dfrac{\partial \varepsilon_D}{\partial r_D}\right]^2}\dfrac{\partial}{\partial r_D}\left[\dfrac{\partial \varepsilon_D}{\partial r_D}\right]+ \\ \dfrac{1}{\dfrac{\partial \varepsilon_D}{\partial r_D}}\dfrac{1}{r_D}- \\ \dfrac{1}{k_D\left[\dfrac{\partial \varepsilon_D}{\partial r_D}\right]^2}\dfrac{\partial \varepsilon_D}{\partial t_D}+ \\ \dfrac{1}{k_D}\dfrac{dk_D}{d\varepsilon_D}\end{array}\right]\frac{dp_D}{d\varepsilon_D}=0 \quad \text{..... (A.17)}$$

The required derivatives of the Boltzmann transform variable (ε_D) are given as follows:

$$\frac{\partial \varepsilon_D}{\partial t_D}=\frac{-1}{t_D}\varepsilon_D \quad \text{..... (A.18)}$$

$$\frac{\partial \varepsilon_D}{\partial r_D}=\frac{2}{r_D}\varepsilon_D \quad \text{..... (A.19)}$$

$$\frac{\partial^2 \varepsilon_D}{\partial r_D^2}=\frac{2}{r_D^2}\varepsilon_D \quad \text{..... (A.20)}$$

Substitution of Eqs. A.18-20 into Eq. A.17 yields,

$$\frac{d^2 p_D}{\partial \varepsilon_D^2} + \left[\begin{array}{c} \dfrac{1}{\left[\dfrac{2\varepsilon_D}{r_D}\right]^2}\left[\dfrac{2\varepsilon_D}{r_D^2}\right] + \\ \dfrac{1}{\dfrac{2\varepsilon_D}{r_D}}\dfrac{1}{r_D} + \\ \dfrac{1}{k_D\left[\dfrac{2\varepsilon_D}{r_D}\right]^2}\dfrac{\varepsilon_D}{t_D} + \\ \dfrac{1}{k_D}\dfrac{dk_D}{d\varepsilon_D} \end{array} \right] \frac{dp_D}{d\varepsilon_D} = 0$$

Cancelling and collecting like terms, we obtain:

$$\frac{d^2 p_D}{d\varepsilon_D^2} + \left[\frac{1}{\varepsilon_D} + \frac{1}{k_D} + \frac{1}{k_D}\frac{dk_D}{d\varepsilon_D}\right]\frac{dp_D}{d\varepsilon_D} = 0 \quad \text{..... (A.21)}$$

Where a slightly more compact form of this result is given by:

$$\frac{d^2 p_D}{d\varepsilon_D^2} + \left[\frac{1}{\varepsilon_D} + \frac{1}{k_D}\left[1 + \frac{dk_D}{d\varepsilon_D}\right]\right]\frac{dp_D}{d\varepsilon_D} = 0 \quad \text{..... (A.22)}$$

At this point we recognize that Eq. A.22 (or A.21) is the fundamental governing relation for fluid flow in our system where the mobility/permeability function is permitted to vary as a function of time and distance. Eq. A.22 is a completely general result — no assumptions have been made at this point.

Our goal is to solve Eq. A.22 for an appropriate set of initial and boundary conditions. The particular case where the Boltzmann transform applies is the case of a uniform initial pres-sure profile in the reservoir (*i.e.*, $p_D(r_D, t_D \leq 0) = 0$) and the case of an "infinite-acting" outer boundary (*i.e.*, $p_D(r_D \rightarrow \infty, t_D) = 0$).

Recalling the definition of the Boltzmann transform variable, ε_D, we have:

$$\varepsilon_D = \frac{r_D^2}{4t_D} \quad \text{..... (A.3)}$$

The initial and outer boundary conditions are expressed in terms of r_D, t_D, and ε_D as follows:

Initial Condition:

$$p_D(r_D, t_D \leq 0) = 0$$
$$\text{for } t_D \rightarrow 0, \varepsilon_D \rightarrow \infty$$
$$p_D(\varepsilon_D \rightarrow \infty) = 0$$

Outer Boundary Condition:

$$p_D(r_D \to \infty, t_D) = 0$$

for $r_D \to \infty, \varepsilon_D \to \infty$

$$p_D(\varepsilon_D \to \infty) = 0$$

We note that in using the Boltzmann transformation, the initial and outer boundary conditions collapse to a single relation:

$$p_D(\varepsilon_D \to \infty) = 0 \quad \text{(A.23)}$$

This result is a unique product of the Boltzmann transformation — *for this particular case*. We will proceed with this result and next we consider the case of a constant flowrate at the well.

Inner Boundary Condition: (Constant Rate)

$$q = \frac{1}{141.2}\frac{kh}{B\mu} r \frac{\partial p}{\partial r} \quad \text{(A.24)}$$

Where Eq. A.23 is written directly from Darcy's law for a radial flow geometry. Isolating the $r(\partial p/\partial r)$ term, we have:

$$r\frac{\partial p}{\partial r} = 141.2\frac{qB\mu}{kh} \quad \text{(A.25)}$$

Substituting the definitions of dimensionless pressure, radius, and permeability (*i.e.*, Eqs. A.6, A.8, and A.11) into Eq. A.25, and rearranging, gives us the following result:

$$\left[r_D \frac{\partial p_D}{\partial r_D} \right]_{r_D} = -\frac{1}{k_D} \quad \text{(A.26)}$$

At the well (*i.e.*, $r=r_w$), we have the cylindrical source form:

$$\left[r_D \frac{\partial p_D}{\partial r_D} \right]_{r_D=1} = -\frac{1}{k_D} \quad \text{(A.27)}$$

However, for our problem we will assume that the well is a mathematical "line source" (*i.e.*, we consider the behavior at $r=0$), this gives:

$$\left[r_D \frac{\partial p_D}{\partial r_D} \right]_{r_D=0} = -\frac{1}{k_D} \quad \text{(A.28)}$$

Using the chain rule and the definition of the Boltzmann trans-form, we obtain the following form of the inner boundary condition:

$$r_D\left[\frac{\partial \varepsilon_D}{\partial r_D}\frac{dp_D}{d\varepsilon_D} \right]_{r_D \to 0} = \left[r_D\left[\frac{2}{r_D}\varepsilon_D \right]\frac{dp_D}{d\varepsilon_D} \right]_{\varepsilon_D \to 0} = -\frac{1}{k_D}$$

Collecting terms gives us:

$$\left[\varepsilon_D \frac{dp_D}{d\varepsilon_D}\right]_{\varepsilon_D \to 0} = -\frac{1}{2}\frac{1}{k_D} \quad \text{..... (A.29)}$$

Recalling our governing relation (*i.e.*, Eq. A.22) we have:

$$\frac{d^2 p_D}{d\varepsilon_D^2} + \left[\frac{1}{\varepsilon_D} + \frac{1}{k_D}\left[1 + \frac{dk_D}{d\varepsilon_D}\right]\right]\frac{dp_D}{d\varepsilon_D} = 0 \quad \text{..... (A.22)}$$

Recalling the unified outer boundary/initial condition (derived using the Boltzmann transform), we have:

$$p_D(\varepsilon_D \to \infty) = 0 \quad \text{..... (A.23)}$$

Recalling the inner boundary condition given in terms of the Boltzmann variable, ε_D, gives us:

$$\left[\varepsilon_D \frac{dp_D}{d\varepsilon_D}\right]_{\varepsilon_D \to 0} = -\frac{1}{2}\frac{1}{k_D} \quad \text{..... (A.29)}$$

In order to develop a solution for Eq. A.22 we will utilize a "variable of transformation" that reduces the differential equation to a more convenient form. At this point we note that Eqs. A.22 and A.29 are only a function of the Boltzmann transform variable, ε_D. As Eq. A.29 is a second order ordinary differential equation, we can surmise that a solution can be obtained by twice integrating the differential equation. This will be our path, but we will also use a variable of transformation to reduce the complexity for the integration of Eq. A.22.

Our "variable of transformation," v, is given as:

$$v = \frac{dp_D}{d\varepsilon_D}$$

where

$$\frac{dv}{d\varepsilon_D} = \frac{d^2 p_D}{d\varepsilon_D^2}$$

Making these substitutions into Eq. A.22 gives us the following "compact form" of the differential equation. We then will solve Eq. A.30 by integration for the v-variable.

$$\frac{dv}{d\varepsilon_D} + \left[\frac{1}{\varepsilon_D} + \frac{1}{k_D}\left[1 + \frac{dk_D}{d\varepsilon_D}\right]\right]v = 0 \quad \text{..... (A.30)}$$

Using Eq. A.15 in the $\frac{1}{k_D}\left[1 + \frac{dk_D}{d\varepsilon_D}\right]$ term from Eq. A.30:

$$\frac{1}{k_D}\left[1 + \frac{dk_D}{d\varepsilon_D}\right] = \frac{1 + ab\,exp[-b\varepsilon_D]}{1 - a\,exp[-b\varepsilon_D]} \quad \text{..... (A.31)}$$

Substituting Eq.A.31 into Eq. A.30 yields,

$$\frac{dv}{d\varepsilon_D} + \left[\frac{1}{\varepsilon_D} + \frac{1 + ab\,exp[-b\varepsilon_D]}{1 - a\,exp[-b\varepsilon_D]}\right]v = 0$$

Isolating/separating the relevant terms we have:

$$\frac{1}{v}dv = -\left[\frac{1}{\varepsilon_D} + \frac{1 + ab\,exp[-b\varepsilon_D]}{1 - a\,exp[-b\varepsilon_D]}\right]d\varepsilon_D \quad \text{..... (A.32)}$$

Setting up the integration of Eq. A.32 gives us:

$$\int \frac{1}{v}dv = -\int\left[\frac{1}{\varepsilon_D} + \frac{1 + ab\,exp[-b\varepsilon_D]}{1 - a\,exp[-b\varepsilon_D]}\right]d\varepsilon_D$$

Expanding the right-hand-side integral gives:

$$\int \frac{1}{v}dv = -\int \frac{1}{\varepsilon_D}d\varepsilon_D - \int \frac{1 + ab\,exp[-b\varepsilon_D]}{1 - a\,exp[-b\varepsilon_D]}d\varepsilon_D$$

Completing the integration, we have:

$$\ln[v] = -\ln[\varepsilon_D] - \int \frac{1 + ab\,exp[-b\varepsilon_D]}{1 - a\,exp[-b\varepsilon_D]}d\varepsilon_D + \beta$$

We note that the β-term is a constant of integration which results from the indefinite integration. The integral that can not be resolved in simple terms must be addressed using tables of integrals, substitution methods, or a symbolic integration product (in this case, we used *Mathematica* (ref. 2)).

From *Mathematica* we obtained the following result for the remaining integral:

$$I = \int \frac{1 + ab\,exp[-b\varepsilon_D]}{1 - a\,exp[-b\varepsilon_D]}d\varepsilon_D$$
$$= -\left[\frac{(1+b)}{b}\ln[e^{-b\varepsilon_D} - a] - b\varepsilon_D\right]$$

Substituting this result into the solution, we have:

$$\ln[v] = -\ln[\varepsilon_D] - \left[\frac{(1+b)}{b}\ln[e^{-b\varepsilon_D} - a] - b\varepsilon_D\right] + \beta$$

Exponentiating the solution, we obtain:

$$v = \frac{\exp[\beta]}{\varepsilon_D}\exp\left[-\left[\frac{(1+b)}{b}\ln[e^{-b\varepsilon_D} - a] - b\varepsilon_D\right]\right]$$

Defining our constant of integration as c_1=exp[β], and substituting this result into the solution, along with the definition v=$dp_D/d\varepsilon_D$, we have:

$$\frac{dp_D}{d\varepsilon_D} = c_1\frac{1}{\varepsilon_D}\exp\left[-\frac{(1+b)}{b}\ln[e^{-b\varepsilon_D} - a] + b\varepsilon_D\right]$$
..... (A.33)

Our next task is to determine the constant of integration, c_1, where this can be accomplished using the inner boundary condition (*i.e.*, Eq., A.29). Multiplying through Eq. A.33 by the Boltzmann transform variable, ε_D, we have:

$$\varepsilon_D \frac{dp_D}{d\varepsilon_D} = c_1 \exp\left[-\left[\frac{(1+b)}{b}\ln[e^{-b\varepsilon_D} - a] - b\varepsilon_D\right]\right]$$

..... (A.34)

Taking the limit of Eq. A.34 as $\varepsilon_D \rightarrow 0$ yields,

$$\lim_{\varepsilon_D \to 0}\left[\varepsilon_D \frac{dp_D}{d\varepsilon_D}\right] = \lim_{\varepsilon_D \to 0}\left[c_1 \exp\left[-\frac{(1+b)}{b}\ln[e^{-b\varepsilon_D} - a] + b\varepsilon_D\right]\right]$$

Which reduces to:

$$\lim_{\varepsilon_D \to 0}\left[\varepsilon_D \frac{dp_D}{d\varepsilon_D}\right] = c_1 \lim_{\varepsilon_D \to 0}\left[\exp\left[\ln[(e^{-b\varepsilon_D} - a)^{-\frac{(1+b)}{b}}]\right]\right]$$

$$= c_1 \lim_{\varepsilon_D \to 0}\left[(e^{-b\varepsilon_D} - a)^{-\frac{(1+b)}{b}}\right]$$

$$= c_1 (1-a)^{-\frac{(1+b)}{b}}$$

Returning to the inner boundary condition, we have:

$$\lim_{\varepsilon_D \to 0}\left[\varepsilon_D \frac{dp_D}{d\varepsilon_D}\right] = \lim_{\varepsilon_D \to 0}\left[-\frac{1}{2}\frac{1}{k_D}\right]$$

$$= -\frac{1}{2}\lim_{\varepsilon_D \to 0}\left[\frac{1}{1 - a\,exp[-b\varepsilon_D]}\right]$$

$$= -\frac{1}{2}\frac{1}{(1-a)}$$

Equating these results:

$$c_1 (1-a)^{-\frac{(1+b)}{b}} = -\frac{1}{2}\frac{1}{(1-a)}$$

And solving for the constant of integration, c_1, we have:

$$\begin{aligned} c_1 &= -\frac{1}{2}\frac{1}{(1-a)}(1-a)^{\frac{(1+b)}{b}} \\ &= -\frac{1}{2}(1-a)^{-1}(1-a)^{\frac{(1+b)}{b}} \\ &= -\frac{1}{2}(1-a)^{\frac{1}{b}} \end{aligned}$$

..... (A.35)

Substitution of the constant of integration, c_1, (Eq. A.35) in the solution (Eq. A.33) gives:

$$\frac{dp_D}{d\varepsilon_D} = -\frac{1}{2}(1-a)^{\frac{1}{b}}\frac{1}{\varepsilon_D}\exp\left[-\frac{(1+b)}{b}\ln[e^{-b\varepsilon_D}-a]+b\varepsilon_D\right]$$

..... (A.36)

Definite integration of Eq. A.36 yields the solution in terms of $p_D(\varepsilon_D)$ — this result is given as:

$$p_D = -\frac{1}{2}(1-a)^{\frac{1}{b}}\int_{\infty}^{\varepsilon_D}\left[\frac{1}{\varepsilon_D}\exp\left[-\frac{(1+b)}{b}\ln[e^{-b\varepsilon_D}-a]+b\varepsilon_D\right]\right]d\varepsilon_D$$

..... (A.37)

Reversing the limits of integration in Eq. A.37 eliminates the (-) sign and puts the result in a more traditional form.

$$p_D = \frac{1}{2}(1-a)^{\frac{1}{b}}\int_{\varepsilon_D}^{\infty}\left[\frac{1}{\varepsilon_D}\exp\left[-\frac{(1+b)}{b}\ln[e^{-b\varepsilon_D}-a]+b\varepsilon_D\right]\right]d\varepsilon_D$$

..... (A.38)

Unfortunately, Eq. A.38 can only be integrated numerically — we have also employed *Mathematica* as the mechanism to compute the numerical integration of Eq. A.38 for the cases considered in this work.

We can, however, use Eq. 36 as given as a mechanism for modelling the pressure derivative behavior in time and radial space. In order to develop these results we require the following identities derived using the chain rule:

$$\frac{dp_D}{d\varepsilon_D} = \frac{\partial t_D}{\partial \varepsilon_D}\frac{\partial p_D}{\partial t_D}$$ ..... (A.39)

$$\frac{dp_D}{d\varepsilon_D} = \frac{\partial r_D}{\partial \varepsilon_D}\frac{\partial p_D}{\partial r_D}$$ ..... (A.40)

Recalling Eqs. A.17 and A.18, we have:

$$\frac{\partial \varepsilon_D}{\partial t_D} = -\frac{1}{t_D}\varepsilon_D \quad \text{..... (A.18)}$$

$$\frac{\partial \varepsilon_D}{\partial r_D} = \frac{2}{r_D}\varepsilon_D \quad \text{..... (A.19)}$$

Substituting Eq. A.18 into Eq. A.39, and solving for $\partial p_D/\partial t_D$, we have:

$$\frac{\partial p_D}{\partial t_D} = \frac{\partial \varepsilon_D}{\partial t_D}\frac{dp_D}{d\varepsilon_D} = -\frac{1}{t_D}\varepsilon_D \frac{dp_D}{d\varepsilon_D}$$

..... (A.41)

Similarly, substituting Eq. A.19 into Eq. A.40, and solving for $\partial p_D/\partial r_D$, we obtain:

$$\frac{\partial p_D}{\partial r_D} = \frac{\partial \varepsilon_D}{\partial r_D}\frac{dp_D}{d\varepsilon_D} = \frac{2}{r_D}\varepsilon_D \frac{dp_D}{d\varepsilon_D}$$

..... (A.42)

The $\partial p_D/\partial t_D$ result is obtained by substitution of Eq. A.36 into Eq. A.41 — this gives:

$$\frac{\partial p_D}{\partial t_D} = \frac{1}{2t_D}(1-a)^{\frac{1}{b}} \exp\left[-\frac{(1+b)}{b}\ln[e^{-b\varepsilon_D} - a] + b\varepsilon_D\right]$$

..... (A.43)

Substituting the definition of the Boltzmann transform variable, $\varepsilon_D = r_D^2/(4t_D)$, into Eq. A.43 gives the final form in terms of r_D and t_D:

$$\frac{\partial p_D}{\partial t_D} = \frac{1}{2t_D}(1-a)^{\frac{1}{b}} \exp\left[-\frac{(1+b)}{b}\ln[e^{-b\frac{r_D^2}{4t_D}} - a] + b\frac{r_D^2}{4t_D}\right]$$

..... (A.44)

The $\partial p_D/\partial r_D$ result is obtained by substitution of Eq. A.36 into Eq. A.42 — this gives:

$$\frac{\partial p_D}{\partial r_D} = -\frac{1}{r_D}(1-a)^{\frac{1}{b}} \exp\left[-\frac{(1+b)}{b}\ln[e^{-b\varepsilon_D} - a] + b\varepsilon_D\right]$$

..... (A.45)

Substituting the definition of the Boltzmann transform variable, $\varepsilon_D = r_D^2/(4t_D)$, into Eq. A.45 gives the final form in terms of r_D and t_D:

$$\frac{\partial p_D}{\partial r_D} = -\frac{1}{r_D}(1-a)^{\frac{1}{b}} \exp\left[-\frac{(1+b)}{b} \ln[e^{-b\frac{r_D^2}{4t_D}} - a] + b\frac{r_D^2}{4t_D} \right] \quad \text{..... (A.46)}$$

Where we recall that the constants *a* and *b* are given by Eqs. A.13 and A.14, respectively:

$$a = (1 - k_{min}/k_{max}) \quad \text{..... (A.13)}$$

$$b = \frac{4}{\alpha_D} \quad \text{..... (A.14)}$$

While we can utilize Eqs. A.44 and A.46 in the given forms, we note that the following forms may be more convenient:

"Pressure Derivative in Time"

$$t_D \frac{\partial p_D}{\partial t_D} = \frac{1}{2}\left[k_{\min}/k_{\max}\right]^{\frac{\alpha_D}{4}} \times \exp\left[-\frac{\left[1+\frac{4}{\alpha_D}\right]}{\frac{4}{\alpha_D}} \ln[e^{-\frac{4}{\alpha_D}\frac{r_D^2}{4t_D}} - (1 - k_{\min}/k_{\max})] + \frac{4}{\alpha_D}\frac{r_D^2}{4t_D} \right] \quad \text{..... (A.47)}$$

And,

"Pressure Derivative in Radial Distance"

$$-r_D \frac{\partial p_D}{\partial r_D} = \left[k_{min}/k_{max}\right]^{\frac{\alpha_D}{4}} \times \exp\left[-\frac{\left[1+\frac{4}{\alpha_D}\right]}{\frac{4}{\alpha_D}} \ln[e^{-\frac{4}{\alpha_D}\frac{r_D^2}{4t_D}} - (1 - k_{min}/k_{max})] + \frac{4}{\alpha_D}\frac{r_D^2}{4t_D} \right] \quad \text{..... (A.48)}$$

Where we recognize that the right-hand-sides (RHS) of Eqs. A.47 and A.48 are identical (except for the 1/2 multiplier in Eq. A.47) — as such, equating Eqs. A.47 and A.48 gives the following identity:

$$2\,t_D \frac{\partial p_D}{\partial t_D} = -r_D \frac{\partial p_D}{\partial r_D} \quad \text{..... (A.49)}$$

We note that the identity given by Eq. A.49 is also obtained for the "homogeneous" case where $k_D = 1$. In fact, for the case of $k_D = 1$, the entire sequence of results reverts to the "traditional" line source solution for a homogeneous, infinite-acting reservoir.

We also note that Eq. A.48 is typically applied as the absolute value of this result for comparative/ illustrative plots (obviously the $\partial p_D/\partial r_D$ term is negative).

Finally, we will also define the dimensionless pressure which includes skin effects as:

$$p_{sD} = p_D + s \quad \text{(A.50)}$$

Where s is the skin factor.

APPENDIX B

AN APPROXIMATE TECHNIQUE FOR THE DIRECT ADDITION OF WELLBORE STORAGE AND SKIN EFFECTS

In this Appendix, we present a simple, approximate technique for adding wellbore storage to dimensionless pressure solutions. This result is taken from Blasingame, *et al.*[17]

The required result from (ref. 4) is given as:

$$p_{wD} = \frac{\psi}{\omega}(1 - \exp[-\omega t_D]) + \frac{\theta}{\omega^2}(\exp[-\omega t_D] + \omega t_D - 1) \quad \text{(B.1)}$$

Where the ω, θ, and ψ parameters in Eq. B.1 are given by:

$$\omega = \frac{1 + C_D \hat{b}}{C_D \hat{a}} \quad \text{(B.2)}$$

$$\psi = \frac{1}{C_D} \quad \text{(B.3)}$$

$$\theta = \frac{\hat{b}}{\hat{a} C_D} \quad \text{(B.4)}$$

Where the $\hat{a}$ and $\hat{b}$ parameters in Eqs. B.2 and B.4 are given by:

$$\hat{a} = p_{sD} - p_{sDd} \quad \text{(B.5)}$$

$$\hat{b} = \frac{dp_{sD}}{dt_D} \quad \text{(B.6)}$$

And,

$$p_{sDd} = t_D \frac{dp_{sD}}{dt_D} \quad \text{(B.7)}$$

Eq. B.1 should provide results which are accurate to within 1-2 percent of the exact solution — for the p_{wD} and the p_{wDd} functions (where $p_{wDd}=t_D(dp_{wD}/dt_D)$).

APPENDIX C

A QUADRATIC FORMULA FOR NUMERICAL DIFFERENTIATION

Presuming a general quadratic polynomial, we have:

$$y = a_0 + a_1 t + a_2 t^2 \quad \text{(C.1)}$$

The coefficients of an interpolating LaGrange collocation polynomial are stated as follows:

$$c_0 = y(t_i) \quad \text{(C.2)}$$

$$c_1 = \frac{y(t_{i-1}) - y(t_i)}{t_{i-1} - t_i} \quad \text{(C.3)}$$

$$c_2 = \frac{y(t_{i-2}) - c_0 - c_1(t_{i-2} - t_i)}{(t_{i-2} - t_i)(t_{i-2} - t_{i-1})} \quad \text{(C.4)}$$

Where we note that we have used a "backward" sampling for the coefficients (*i.e.*, in terms of t_i, t_{i-1}, and t_{i-2}) — this is for convenience in our present work. Alternatively, we could use forward or central sampling with no loss in generality.

The a_0, a_1, and a_2 coefficients for Eq. C.1 are defined in terms of the coefficients of the collocation polynomial as follows:

$$a_0 = c_0 - c_1 t_i + c_2 t_i t_{i-1} \quad \text{(C.5)}$$

$$a_1 = c_1 - c_2(t_i + t_{i-1}) \quad \text{(C.6)}$$

$$a_2 = c_2 \quad \text{(C.7)}$$

The derivative of Eq. C.1 is:

$$\frac{dy}{dt} = a_1 + 2a_2 t \quad \text{(C.8)}$$

Given a table of t and $y(t)$ values, Eqs. C.2-C.7 are used to compute the required coefficients. Eq. C.8 is used to compute the desired derivative.

VITA

Name:	Benton Wade Wilson
Born:	18 September 1964 Shreveport, Louisiana (United States of America)
Permanent Address:	27210 Cherokee Lane Magnolia, TX 77354 United States of America (wade.wilson@bakeratlas.com)
Education:	Georgia Institute of Technology Bachelor of Science Degree in Civil Engineering July 1991
	Texas A&M University, College Station, Texas, USA Master of Science Degree in Petroleum Engineering December 2003